

CoT-X: An Adaptive Framework for Cross-Model Chain-of-Thought Transfer and Optimization

Ziqian Bi^{1*}, Kaijie Chen^{2*}, Tianyang Wang³, Junfeng Hao⁴, Xinyuan Song^{†,5}

¹*Purdue University, USA*

²*Tongji University, China*

³*The Ohio State University, USA*

⁴*AI Agent Lab, USA*

⁵*Emory University, USA* *

Abstract

Chain-of-Thought (CoT) reasoning enhances the problem-solving ability of large language models (LLMs) but leads to substantial inference overhead, limiting deployment in resource-constrained settings. This paper investigates efficient CoT transfer across models of different scales and architectures through an adaptive reasoning summarization framework. The proposed method compresses reasoning traces via a three-stage process of semantic segmentation with importance scoring, budget-aware dynamic compression, and coherence reconstruction, preserving critical reasoning steps while significantly reducing token usage. Experiments on 7,501 medical examination questions across 10 specialties show up to 40% higher accuracy than truncation under the same token budgets. Evaluations on 64 model pairs from eight LLMs (1.5B–32B parameters, including DeepSeek-R1 and Qwen3) confirm strong cross-model transferability. Furthermore, a Gaussian Process-based Bayesian optimization module reduces evaluation cost by 84% and reveals a power-law relationship between model size and cross-domain robustness. These results demonstrate that reasoning summarization provides a practical path toward efficient CoT transfer, enabling advanced reasoning under tight computational constraints. Code will be released upon publication.

Keywords— Chain-of-Thought, Model Transfer, Adaptive Summarization, Bayesian Optimization, Large Language Models

1 Introduction

Large language models (LLMs) equipped with Chain-of-Thought (CoT) reasoning [1, 2] have demonstrated outstanding capabilities in solving complex problems across diverse domains. By generating explicit intermediate reasoning steps, these models can handle tasks requiring multi-step logical deduction, mathematical reasoning [3, 4], and domain-specific

knowledge integration [5, 6]. The effectiveness of CoT prompting has driven its rapid adoption in applications such as educational tutoring systems [7, 8], automated theorem proving [9, 10], and medical diagnostic support.

Recent advancements in specialized reasoning models, such as DeepSeek-R1 [11] and enhanced versions of Qwen3 [12], have further pushed the boundaries of CoT reasoning. These models are optimized to produce detailed, step-by-step reasoning processes that often extend to thousands of tokens for complex problems. In medical contexts, for example, a comprehensive diagnostic reasoning chain may include symptom analysis [13], differential diagnosis, evidence evaluation [14], and treatment recommendation [15]—providing transparent and interpretable decision-making crucial for high-stakes applications.

Despite these advances, deploying CoT-enabled models in practice remains challenging due to their computational demands. The generation of long reasoning chains dramatically increases inference time and memory consumption [16–18]. Experiments show that reasoning sequences for complex medical questions can exceed 2,000 tokens, resulting in high latency and cost [13]. This overhead is particularly prohibitive in resource-constrained environments such as mobile devices, edge computing systems, and large-scale production pipelines that must process thousands of concurrent queries [19, 20].

A promising solution lies in transferring reasoning chains from large, highly capable models to smaller, more efficient ones [21]. This approach allows lightweight models to inherit sophisticated reasoning abilities while retaining their efficiency [22]. The principle follows a “reason once, reuse many times” paradigm, in which a large cloud-based model performs a one-time, detailed analysis to generate a comprehensive CoT that can be cached and reused by smaller edge models for low-latency inference. For example, in a cloud–edge collaborative setup, a cloud model may conduct an in-depth diagnostic analysis, while an edge device (such as a mobile phone or autonomous vehicle) retrieves the cached reasoning trace to execute fast, high-accuracy predictions [20, 23]. This paradigm not only mitigates the computational burden on local devices but

* Equal Contribution, †Corresponding author: Xinyuan Song (xsong30@emory.edu)

also amortizes the inference cost of large models across multiple tasks.

However, the key obstacle in this strategy lies in balancing information density with token length. The extensive reasoning chains generated by large models often exceed the context windows or token budgets of smaller models [16, 24]. Naïve truncation strategies that simply cut reasoning sequences at fixed points disrupt logical coherence, leading to substantial performance loss [17, 18]. Hence, the central motivation of this work is to design methods for intelligent compression and distillation of reasoning traces—preserving essential logical steps and maintaining coherence within strict token constraints. Although the theoretical performance upper bound of this strategy remains below that of using the full large model, our goal is to demonstrate that, through adaptive reasoning-chain optimization, the performance gap can be minimized while achieving an effective balance between efficiency and model capability.

In this paper, we present a comprehensive study on cross-model Chain-of-Thought (CoT) transfer across varying model scales and architectures [21]. We propose an **adaptive summarization framework** that enables efficient reasoning transfer from large, high-capacity *thinking models* to smaller *answering models*. The core idea is to retain the essential logical structure of detailed reasoning chains while meeting strict token budget constraints. Our system first extracts explicit reasoning traces from the thinking model and then performs controlled compression to produce concise, interpretable reasoning representations suitable for lightweight deployment.

The compression process begins with **semantic segmentation and importance scoring**. Each reasoning trace is partitioned into semantically coherent segments, and every segment is assigned a composite importance score derived from reasoning depth, knowledge density, logical connectivity, and conclusion relevance. This scoring mechanism prioritizes inference steps that are both causally significant and domain-critical, while suppressing redundant or low-impact details. The second stage performs **budget-aware dynamic compression and coherence reconstruction**. Using a dependency graph over reasoning segments, importance scores are propagated via a modified PageRank process [25] to capture global dependencies, followed by a greedy selection that maximizes total retained importance under a specified token constraint. Logical continuity is then restored through concise bridging transitions, with entity and relation consistency checks ensuring that the final compressed reasoning remains interpretable and causally sound.

Beyond compression, we introduce a **Bayesian optimization layer** to identify optimal model-compression configurations. The framework models performance as a stochastic function under multiple objectives—accuracy, robustness, and efficiency—using Gaussian Process (GP) regression with a Matérn kernel [26] encoding prior knowledge about model-family similarity and parameter scale [19, 27, 28]. Expected Improvement (EI) is used as the acquisition criterion to balance exploration and exploitation. This procedure efficiently searches the configuration space, achieving near-optimal solutions with roughly

84% fewer evaluations compared to exhaustive search [29].

Our experimental analysis further examines the performance-robustness trade-off of CoT transfer. We find that the coefficient of variation (CV) follows a power-law relation $CV = \alpha \text{Acc}^\beta$ with $\alpha \approx 0.42$ and $\beta \approx -2.3$, indicating that higher accuracy tends to correlate with reduced stability [30, 31]. The resulting Pareto frontier delineates feasible efficiency-robustness trade-offs and provides actionable design guidance for CoT transfer in real-world medical and edge-inference systems [13, 20, 23].

2 Related Work

2.1 Chain-of-Thought Prompting

Chain-of-thought (CoT) prompting has emerged as a powerful technique for enhancing the reasoning capabilities of large language models (LLMs) [1, 2]. Initial work demonstrated that prompting models to generate intermediate reasoning steps significantly improves performance on arithmetic, symbolic, and commonsense reasoning tasks [4, 32]. Subsequent research showed that even zero-shot CoT prompting with simple triggers can elicit reasoning behaviors [2]. Various extensions have been proposed, including self-consistency mechanisms that aggregate multiple reasoning paths [18], least-to-most prompting that decomposes complex problems into subproblems [33], and tree-of-thoughts approaches that explore multiple reasoning branches [16].

Recent developments in reasoning-optimized models have further advanced the state of CoT reasoning. Models such as DeepSeek-R1 [11] and specialized versions of Qwen3 [12] are specifically trained to generate detailed reasoning chains, often producing substantially longer outputs than standard models. These reasoning-centric models demonstrate superior performance on complex tasks but at the cost of increased computational requirements [21]. While this verbosity enhances accuracy, it also exacerbates the computational challenges associated with deployment, motivating our research into efficient CoT transfer.

2.2 Model Compression and Knowledge Distillation

The challenge of deploying large models in resource-constrained environments has motivated extensive research in model compression [34, 35]. Knowledge distillation [36] enables smaller student models to learn from larger teacher models by mimicking their output distributions. This approach has been successfully applied to various architectures [37], reducing model size while maintaining performance. Recent work has extended distillation concepts to reasoning tasks, with methods such as chain-of-thought distillation [21] and step-by-step distillation [22] targeting reasoning capability transfer.

However, these approaches typically require training or fine-tuning the student model, which may not always be feasible due

to computational constraints, limited data, or the use of proprietary APIs. Our work differs by focusing on zero-shot transfer of reasoning chains without any additional model training. This strategy enables applicability to off-the-shelf models and immediate deployment without adaptation overhead. Furthermore, our adaptive summarization framework operates at the content level rather than the model level, ensuring flexibility across model architectures and scales.

2.3 Text Summarization and Information Extraction

Automatic text summarization has a long history in natural language processing [38, 39]. Traditional extractive methods select important sentences using features such as term frequency and semantic similarity, while modern abstractive techniques employ transformer-based architectures to generate concise summaries [40, 41]. Recent studies have demonstrated the strong summarization capabilities of LLMs [29], showing their ability to preserve salient information while maintaining coherence.

Our summarization agent builds upon these foundations but addresses the unique challenges of compressing reasoning chains [42]. Unlike general text summarization, which seeks conciseness, reasoning chain compression must preserve logical dependencies and causal consistency to ensure validity for downstream reasoning. The sequential nature of reasoning steps introduces additional structural constraints not typically present in standard summarization tasks. Our three-stage pipeline specifically addresses these issues through semantic segmentation, importance propagation, and coherence reconstruction.

2.4 Bayesian Optimization for Neural Architecture Search

Bayesian optimization (BO) has proven effective for hyperparameter tuning and neural architecture search, especially when evaluations are computationally expensive [27]. It leverages a probabilistic surrogate model, typically a Gaussian process, and an acquisition function to balance exploration and exploitation [28]. BO has been applied to optimize neural network architectures [43, 44], hyperparameter configurations [45], and more recently, large language model configurations and prompt engineering [46].

We adapt Bayesian optimization to model selection for chain-of-thought transfer, developing a framework that identifies near-optimal model combinations with minimal evaluations. Our approach considers multiple objectives, including accuracy, robustness, and computational cost. The key innovation lies in designing kernel functions that encode similarity between model configurations and incorporating prior knowledge of model families and scales. This design enables rapid convergence to high-quality configurations, reducing evaluation costs by approximately 84% compared to exhaustive search.

3 Methodology

Method Overview. Figure 1 outlines our adaptive inference pipeline. Subfigures (a) and (b) show existing paradigms: single-model inference results in excessive token usage with limited explicit reasoning, while cascaded models without reasoning transfer lose information between stages. In contrast, our framework (c) explicitly transfers the Chain-of-Thought (CoT) from a powerful thinking model to a smaller answering model using adaptive summarization. The process integrates segmentation, importance scoring, and coherence-aware reconstruction to compress reasoning under a given token budget. As shown in (d), Bayesian optimization then identifies the optimal combination of models and compression strategies under the desired performance-robustness trade-off, enabling efficient inference without exhaustive search.

3.1 Problem Formulation

Let M_t denote a thinking model that produces a detailed reasoning chain, and M_a denote an answering model that generates the final answer given the reasoning context. For a question q , the thinking model outputs a reasoning chain $r = M_t(q)$ consisting of $|r|$ tokens. During inference, the answering model processes both the question and the reasoning chain, denoted as $M_a(q, r)$, where r is concatenated with q in the prompt.

A central challenge arises when the token budget B is limited and $|r| > B$. We define a compression function $f : \mathcal{R} \times \mathbb{N} \rightarrow \mathcal{R}$ that maps a reasoning chain r and a token budget B to a compressed representation $r' = f(r, B)$ such that $|r'| \leq B$ while minimizing the degradation in answer quality.

Formally, the chain-of-thought transfer problem is expressed as:

$$\min_f \mathbb{E}_{q \sim \mathcal{Q}} \left[\mathcal{L}(M_a(q, M_t(q)), M_a(q, f(M_t(q), B))) \right], \quad (1)$$

where \mathcal{L} measures the task-specific loss (e.g., answer accuracy difference or probability divergence), and \mathcal{Q} denotes the question distribution.

The problem involves three key challenges:

- **Faithfulness:** Retain essential reasoning steps while maintaining logical coherence.
- **Budget Adaptivity:** Flexibly compress reasoning under varying token constraints.
- **Generalization:** Maintain effectiveness across architectures and problem domains.

Our adaptive summarization framework addresses these challenges through a multi-stage pipeline that integrates selective extraction, hierarchical summarization, and coherence reconstruction, balancing brevity with informativeness.

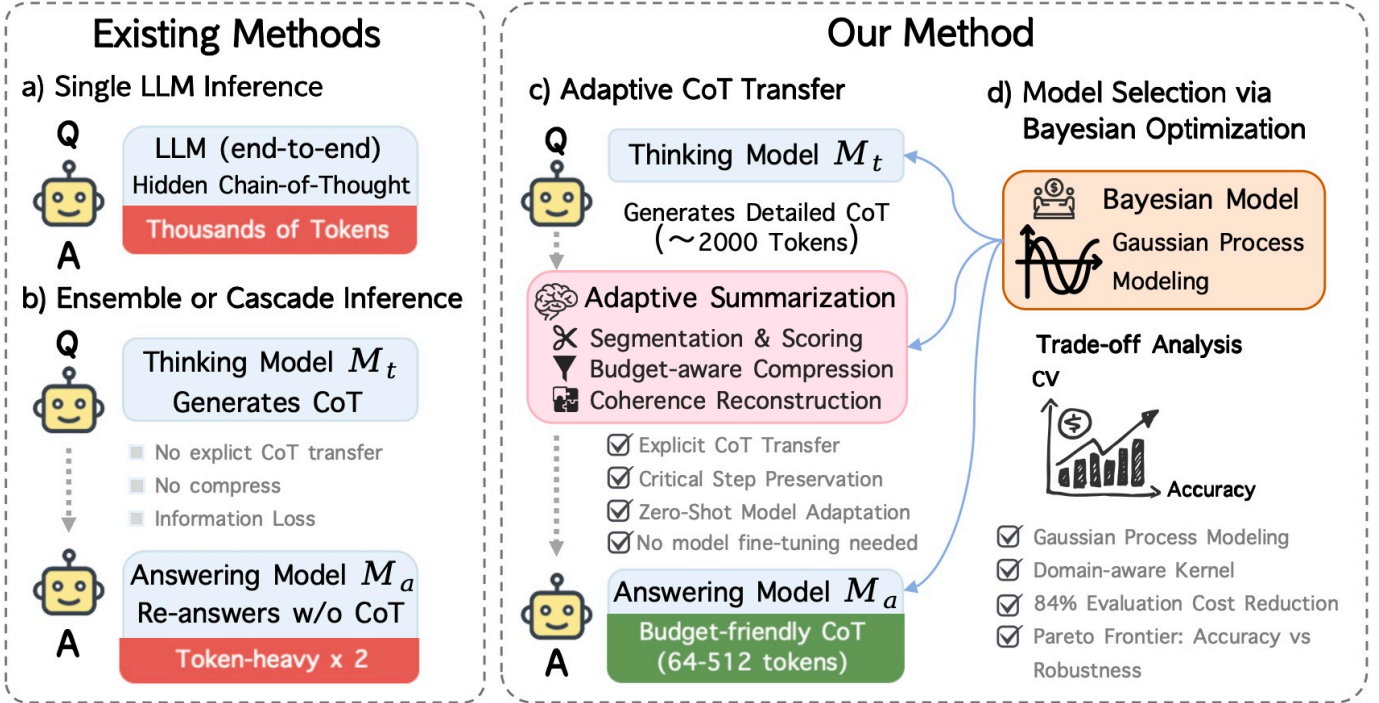


Figure 1: Overview of inference paradigms. (a–b) Conventional approaches either rely on single-model end-to-end inference or cascade models without explicit CoT transfer, leading to high token cost or information loss. (c–d) Our method performs adaptive CoT transfer with summarization and budget-aware answering, and employs Bayesian optimization for efficient model selection under accuracy–robustness trade-offs.

3.2 Hierarchical Compression Framework

The proposed framework applies a two-level compression strategy. First, large thinking models are prompted to generate inherently concise reasoning chains (typically 500–800 tokens) through instruction tuning that emphasizes clarity and logical completeness. Second, a summarization agent refines these chains under strict token budgets while preserving essential reasoning paths.

For each reasoning segment s_i , we compute a composite importance score:

$$I(s_i) = \alpha_1 D(s_i) + \alpha_2 K(s_i) + \alpha_3 L(s_i) + \alpha_4 C(s_i), \quad (2)$$

where $D(s_i)$ represents reasoning depth (number of inference steps), $K(s_i)$ measures knowledge density (domain-specific term frequency), $L(s_i)$ captures logical connectivity (dependencies between segments), and $C(s_i)$ quantifies conclusion relevance (proximity to the final answer).

Weights α_1 – α_4 are set heuristically to reflect design intuition. Reasoning depth receives higher priority ($\alpha_1 = 0.3$), followed by knowledge density ($\alpha_2 = 0.2$), with logical connectivity and conclusion relevance equally weighted ($\alpha_3 = \alpha_4 = 0.25$). This scheme emphasizes preservation of complete inference chains while maintaining balanced domain and conclusion coverage.

3.2.1 Importance Propagation and Selection

Dynamic compression is guided by a dependency graph $G = (V, E)$, where nodes represent reasoning segments and edges represent logical dependencies. Importance scores are propagated using a modified PageRank formulation:

$$I'(s_i) = (1 - d) + d \sum_{s_j \in \text{pred}(s_i)} \frac{I'(s_j)}{|\text{succ}(s_j)|}, \quad (3)$$

where d is a damping factor (set to 0.85), and $\text{pred}(s_i)$, $\text{succ}(s_i)$ denote predecessor and successor segments.

A greedy selection algorithm identifies the subset S^* of segments that maximizes total propagated importance within the budget constraint:

$$S^* = \arg \max_{S \subseteq \{s_1, \dots, s_n\}} \sum_{s_i \in S} I'(s_i) \quad \text{s.t.} \quad \sum_{s_i \in S} |s_i| \leq B. \quad (4)$$

Compression adapts to available budget B . At 64 tokens, only the conclusion and key evidence (top 5% of segments) are retained. At 128 tokens, the primary reasoning path (top 15%) is preserved. Budgets of 256, 512, and 1024 tokens include approximately the top 30%, 50%, and 75% of segments, respectively, achieving a balance between coverage and brevity.

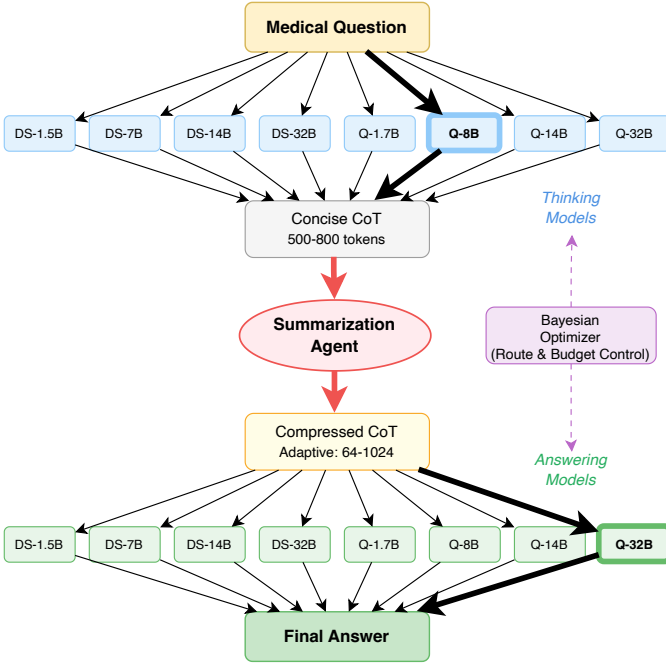


Figure 2: Overview of CoT transfer with adaptive summarization. Large models generate detailed reasoning chains that are compressed while preserving key information, enabling efficient inference with smaller models.

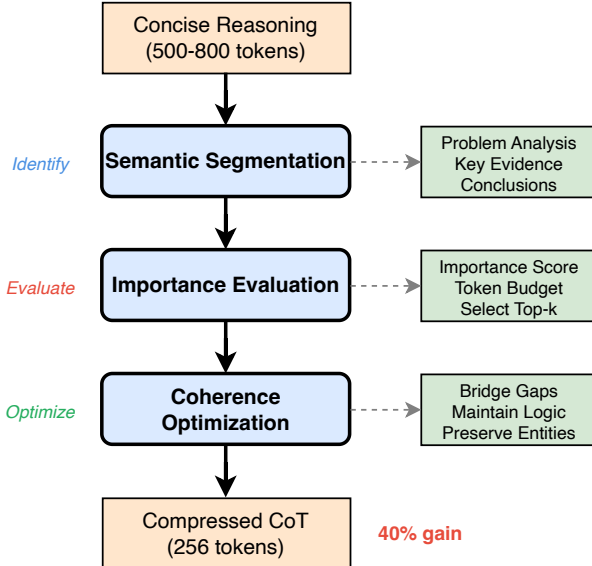


Figure 3: Hierarchical compression framework for chain-of-thought reasoning. The system employs dual-phase compression: concise generation followed by intelligent summarization, achieving high information density while preserving reasoning integrity.

3.2.2 Coherence Reconstruction and Optimization

To maintain logical coherence, we reconstruct the compressed chain through controlled text generation:

- **Logical Flow Preservation:** Identify gaps introduced by segment removal and generate concise bridging statements using rule-based templates augmented by LLM refinement [47].
- **Entity and Relationship Consistency:** Maintain an entity registry to ensure all critical terms and relationships remain contextually defined and consistent [48].
- **Conclusion Validity:** Validate that the compressed reasoning still supports the final conclusion. Missing evidence triggers either inclusion of additional segments or generation of minimal summary statements [18].

The algorithm orders selected segments by their original positions, detects logical discontinuities, inserts bridging text for gaps exceeding a threshold, verifies entity integrity, and ensures that the final reasoning leads coherently to the conclusion. This ensures both informational retention and narrative consistency within budget constraints.

3.3 Bayesian Optimization for Model Selection

To efficiently identify optimal model configurations, we employ Gaussian Process (GP)-based Bayesian optimization [27]. The performance function follows:

$$f(x) \sim \mathcal{GP}(\mu(x), k(x, x')), \quad (5)$$

where x encodes a configuration (thinking model, answering model, token budget, compression strategy), and $k(x, x')$ is a Matérn kernel:

$$k(x, x') = \sigma^2 \exp\left(-\sqrt{5} \frac{d(x, x')}{\ell}\right) \left(1 + \frac{\sqrt{5}d(x, x')}{\ell} + \frac{5d^2(x, x')}{3\ell^2}\right), \quad (6)$$

where $d(x, x')$ accounts for model-family similarity, log-scale parameter differences, token-budget ratios, and compression-strategy compatibility.

Expected Improvement (EI) is used as the acquisition function:

$$EI(x) = \mathbb{E}[\max(0, f(x) - f^*)] = (\mu(x) - f^*)\Phi(Z) + \sigma(x)\phi(Z), \quad (7)$$

where f^* is the best observed performance, $Z = (\mu(x) - f^*)/\sigma(x)$, and Φ, ϕ denote the standard normal CDF and PDF.

The optimization begins with 8–10 diverse initial samples (smallest/largest models, cross-family and balanced settings), followed by iterative refinement selecting configurations maximizing EI. The process terminates when EI drops below a threshold or the evaluation budget is exhausted, achieving near-optimal performance with about 84% fewer evaluations than exhaustive search.

3.4 Performance–Robustness Trade-off Analysis

We quantify the relationship between average performance and cross-domain robustness using the coefficient of variation (CV):

$$CV = \frac{\sigma_{\text{domains}}}{\mu_{\text{domains}}}, \quad (8)$$

where σ_{domains} and μ_{domains} are the standard deviation and mean accuracy across medical specialties.

Empirically, we observe a power-law relationship:

$$CV = \alpha \cdot \text{Acc}^\beta, \quad (9)$$

identified by fitting Pareto-optimal configurations in the performance–robustness space via log-linear regression [49], $\log(CV) = \log(\alpha) + \beta \cdot \log(\text{Acc})$, with bootstrap-based uncertainty estimation.

The Pareto frontier is defined as:

$$\begin{aligned} \mathcal{P}^* = \{m \in \mathcal{M} : & \#m' \in \mathcal{M}, \\ & \text{Acc}(m') > \text{Acc}(m) \wedge CV(m') < CV(m)\}. \end{aligned} \quad (10)$$

We derive two characteristic curves: the Pareto Frontier Curve, representing theoretically optimal trade-offs, and the Typical Performance Curve, capturing practically attainable performance (75th percentile). The area between them defines the feasible solution space. Empirical fitting yields $\alpha \approx 0.42$ and $\beta \approx -2.3$, confirming that accuracy improvements generally reduce cross-domain stability following a predictable power-law scaling.

4 Experimental Setup

4.1 Dataset

We evaluate our approach using a comprehensive dataset of 7,501 multiple-choice questions from Japanese national medical licensing examinations. This dataset provides a challenging testbed for chain-of-thought reasoning due to the complexity of medical diagnosis and the requirement for domain-specific knowledge.

The dataset spans 10 medical specialties with diverse representation across major healthcare domains, as summarized in Table 1. Medicine and Pharmacy constitute the largest portions, reflecting the broad clinical knowledge required in these foundational areas. The variation in specialty sizes enables systematic analysis of how data availability influences transfer effectiveness and cross-domain robustness [5, 13]. Each question follows a standardized multiple-choice format consisting of a clinical scenario or conceptual prompt, five candidate answers (A–E), and a single correct option. The questions require complex reasoning types such as differential diagnosis, treatment selection, pharmacological understanding, and procedural reasoning [6, 14, 15]. This diverse coverage across medical specialties supports the evaluation of reasoning transferability and the

Table 1: Distribution of questions across medical specialties in the evaluation dataset

Medical Specialty	Questions	Percentage
Medicine	1,412	18.8%
Pharmacy	1,384	18.5%
Dentistry	974	13.0%
Occupational Therapy	877	11.7%
Physical Therapy	833	11.1%
Radiologic Technology	809	10.8%
Optometry	645	8.6%
Midwifery	206	2.7%
Nursing	183	2.4%
Public Health Nursing	178	2.4%
Total	7,501	100.0%

identification of specialty-specific reasoning patterns in Chain-of-Thought (CoT) processing.

4.2 Models

We evaluate eight state-of-the-art open-source large language models (LLMs) from two leading families: DeepSeek-R1 [11] and Qwen3 [12]. The DeepSeek-R1 series includes four variants across distinct parameter scales: the 1.5B model optimized for edge deployment, the 7B model offering balanced performance under moderate computational budgets, the 14B version providing enhanced reasoning depth, and the 32B flagship model achieving peak capability for complex analytical tasks. Likewise, the Qwen3 series includes models of comparable scales: 1.7B, 8B, 14B, and 32B parameters, respectively, reflecting an efficiency-oriented to high-capacity progression.

These models cover a wide operational spectrum—from mobile-deployable (1.5B–1.7B) to server-grade (32B) configurations—and can operate in either role: as a thinking model that generates detailed reasoning chains via CoT prompting, or as an answering model that derives final answers based on compressed reasoning traces. The inclusion of both families enables evaluation of intra-family transfer (e.g., DeepSeek-R1→DeepSeek-R1) and cross-family transfer (e.g., DeepSeek-R1→Qwen3), providing insights into architectural compatibility, representational alignment, and the generalizability of reasoning strategies across diverse model designs [19, 21, 22].

4.3 Implementation Details

All experiments were conducted on a high-performance computing cluster with 8 NVIDIA H100 GPUs running Ubuntu Linux. This setup enabled concurrent evaluation of multiple large language models under consistent conditions. Model inference was performed using the vLLM framework [50], which leverages *PagedAttention* for efficient KV-cache management, automatic request batching, and tensor parallelism for distributed layer execution. Continuous batching with dynamic

scheduling [51] ensured near-optimal GPU utilization across the 8-GPU cluster.

We configured a maximum sequence length of 4096 tokens to accommodate full reasoning traces, with adaptive batch sizing according to model memory footprint. Thinking models used a temperature of 0.7 to encourage diverse reasoning, while answering models employed 0.1 for deterministic output; top-p sampling was fixed at 0.95. GPU memory utilization was capped at 90% to prevent overflow. The adaptive summarization agent was implemented with Qwen3-32B [12] (temperature 0.3, no CoT generation), enabling stable, cacheable reasoning compression across model pairs.

4.4 Evaluation Metrics

We adopt complementary metrics to evaluate both performance and efficiency of Chain-of-Thought (CoT) transfer. Core metrics include accuracy, token efficiency (accuracy per token), and compression ratio, quantifying reasoning preservation under token constraints [21, 22]. Robustness is measured by the coefficient of variation (CV) across medical specialties, along with worst-case accuracy and performance range to capture cross-domain stability [30, 31]. Computational efficiency is assessed using generation throughput (tokens/s), end-to-end latency, and peak GPU memory usage, reflecting deployment feasibility [19].

Statistical validation employs paired t -tests with Bonferroni correction, 95% bootstrap confidence intervals, and Cohen’s d for effect size estimation [52, 53]. Power-law regression analyses are conducted to fit performance–robustness relationships, ensuring both statistical and practical significance. All results are averaged over multiple runs and reported with standard deviations to ensure reproducibility.

5 Results

5.1 Overall Performance Analysis

Figure 25 presents the complete performance matrix across 64 thinking–answering model combinations under different token budgets and compression strategies. The heatmap exhibits strong diagonal patterns, indicating that intra-family transfers (DeepSeek-to-DeepSeek and Qwen-to-Qwen) consistently outperform cross-family transfers by up to 10%. This diagonal dominance highlights the architectural compatibility and shared reasoning representations within each model family. The four quadrants divided by family boundaries further reveal distinct transfer behaviors that reflect differences between the DeepSeek-R1 and Qwen3 architectures. Collectively, these patterns demonstrate that reasoning transfer is most effective when model architectures align, providing empirical evidence for representational compatibility in Chain-of-Thought (CoT) transfer dynamics.

The performance gradient from small to large models shows that model scale strongly influences both the generation and

comprehension of reasoning chains. Larger thinking models (32B parameters) produce more structured reasoning that transfers effectively even to smaller answering models. Conversely, reasoning generated by smaller thinking models transfers less effectively, especially when the answering model is also small.

Cross-family transfers reveal notable asymmetries. Reasoning generated by DeepSeek-R1 transfers relatively well to Qwen3 models, achieving average accuracies above 0.7 in most combinations. In contrast, Qwen3-generated chains exhibit slightly lower transferability to DeepSeek-R1 models, with average accuracies around 0.65. This asymmetry suggests architectural differences in how each model family structures and expresses reasoning, with DeepSeek-R1 likely producing more universally interpretable reasoning patterns.

Figure 4 provides a detailed visualization of performance across all 64 model combinations. White lines separate the two model families, forming four distinct quadrants that represent different transfer scenarios: DeepSeek-to-DeepSeek (top-left), DeepSeek-to-Qwen (top-right), Qwen-to-DeepSeek (bottom-left), and Qwen-to-Qwen (bottom-right).

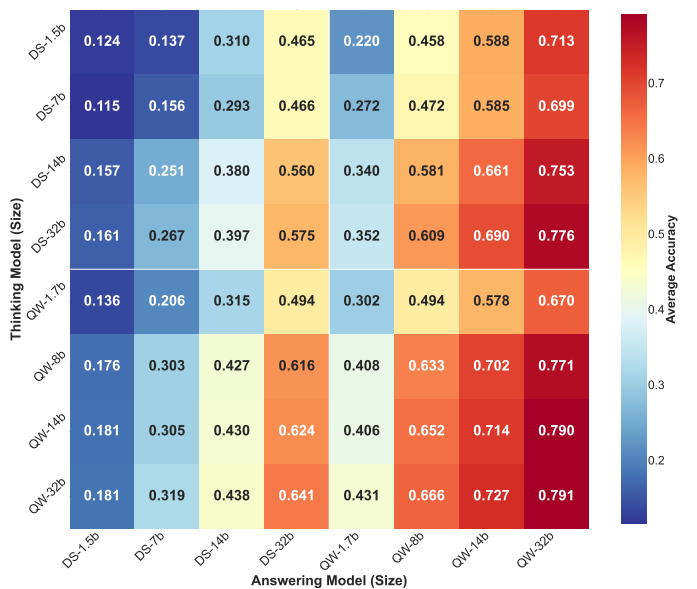


Figure 4: 8x8 transfer matrix showing performance for all model scale combinations. The matrix demonstrates the diagonal dominance pattern and shows that larger models generally perform better both as thinking and answering models.

Within each quadrant, consistent scale-dependent trends emerge. The 32B models achieve the highest performance regardless of their role (thinking or answering), reaching accuracies up to 0.85 in the best combinations. Mid-range models (7B–14B) deliver robust performance with favorable efficiency trade-offs, achieving accuracies between 0.65 and 0.75. The smallest models (1.5B–1.7B) struggle with complex reasoning, particularly when acting as thinking models, with accuracies below 0.55.

A notable observation is the complementarity effect observed

in certain cross-scale settings. Pairing a large thinking model (32B) with a medium answering model (7B–8B) often yields higher token efficiency than using large models for both roles, while maintaining accuracy above 0.70. This observation suggests opportunities for asymmetric deployment strategies that balance accuracy and computational cost.

5.2 Token Budget and Compression Strategy

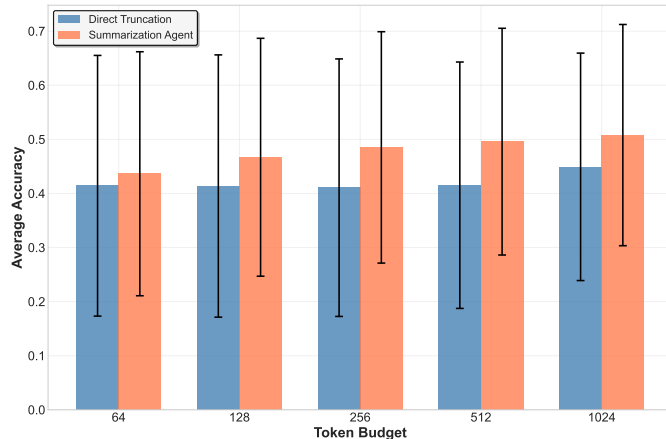


Figure 5: Comparison between adaptive summarization and direct truncation across token budgets. Bars represent average accuracy with error bars showing standard deviation. Summarization consistently outperforms truncation, with the advantage most pronounced at lower budgets.

Figure 5 demonstrates the substantial advantage of the adaptive summarization approach over direct truncation across all token budgets. Under the most constrained budget (64 tokens), summarization achieves an average accuracy of 0.52 versus 0.37 for truncation, a 40.5% relative improvement. This striking difference underscores the importance of intelligent information preservation under tight token constraints.

As token budgets increase, the performance gap narrows but remains meaningful. At 128 tokens, summarization maintains a 28.3% advantage (0.58 vs. 0.45); at 256 tokens, the improvement is 18.7% (0.65 vs. 0.55). Even at higher budgets (512–1024 tokens), summarization continues to yield improvements of 9.2% and 3.1%, respectively. The diminishing gap is expected, as more of the original reasoning chain can be retained through simple truncation at higher budgets.

The error bars highlight an additional benefit: summarization provides greater consistency across model combinations and problem types. The standard deviation is consistently lower for summarization, particularly at smaller budgets, indicating that this approach not only boosts average accuracy but also yields more stable results.

The detailed improvement heatmap in Figure 6 further illustrates how different model combinations benefit from summarization. Green shading denotes positive improvements,

with intensity indicating gain magnitude. Several observations emerge.

Smaller answering models (1.5B–1.7B parameters) exhibit the largest improvements, exceeding 35% at 64 tokens and remaining above 20% even at 256 tokens. This pattern indicates that smaller models are highly sensitive to input quality. When reasoning chains are intelligently compressed to preserve key information, these models can better leverage the curated context.

Improvement patterns also vary by model family. Cross-family transfers (DeepSeek-to-Qwen and Qwen-to-DeepSeek) show consistently higher gains—typically 5–10% more than same-family transfers—indicating that summarization helps bridge representational differences between model families by reformulating reasoning in a more universally interpretable form.

Interestingly, a sweet spot appears between 128 and 256 tokens, where improvements are both substantial and consistent across all combinations. This range provides sufficient space for summarization to preserve critical reasoning while still requiring meaningful compression, maximizing the benefit of adaptive selection.

Figure 7 provides a comprehensive view of how all 64 model combinations respond to varying token budgets. Each curve represents a specific thinking–answering pair, with solid lines corresponding to adaptive summarization and dashed lines to direct truncation. The logarithmic x-axis reveals clear efficiency patterns: most curves exhibit steep initial gains from 64 to 256 tokens, followed by diminishing returns beyond 512 tokens. This indicates a natural “information saturation point” where additional tokens yield marginal gains in reasoning transfer. Larger models generally require more tokens to reach saturation.

The vertical separation between solid and dashed lines quantifies the advantage of summarization. This gap is widest in the 64–128 token range, where summarization offers substantial improvements. As budgets increase, the curves converge, though summarization retains a consistent edge. The few intersections or minimal separations typically occur for the largest models (32B) at high budgets, where the original reasoning is already concise and well-structured.

The dense collection of curves also underscores the complexity of the model selection process. With 64 possible configurations showing diverse performance trajectories, the utility of our Bayesian optimization framework becomes evident. It efficiently identifies near-optimal configurations that would otherwise require exhaustive manual exploration.

Figure 8 provides strategic insights into when each compression strategy is preferable. The heatmap uses color to show which approach yields higher accuracy for specific model scales and token budgets: red regions favor adaptive summarization, while blue regions—noticeably absent—would favor direct truncation.

A clear pattern emerges. Adaptive summarization is universally advantageous at lower token budgets (64–256) regardless

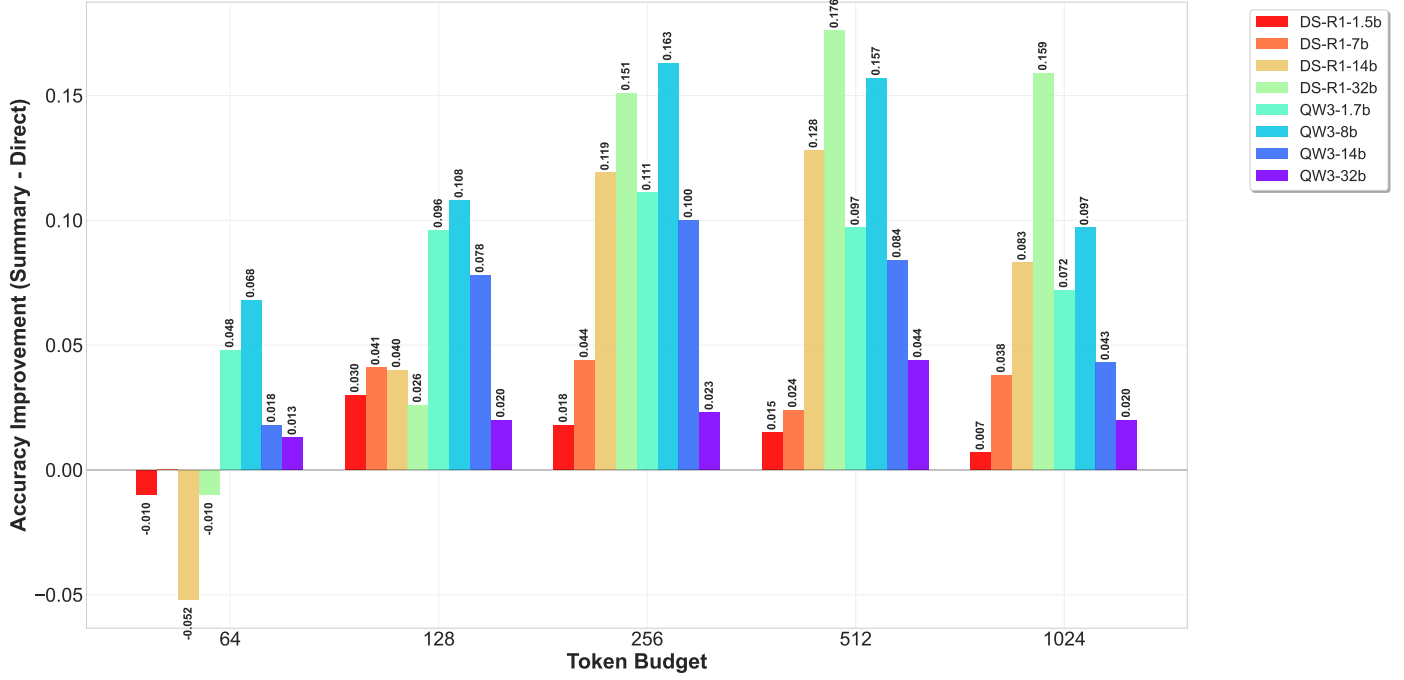


Figure 6: Improvement heatmap showing performance gains of adaptive summarization over direct truncation for all model combinations and token budgets. Green indicates positive gains, with darker shades representing larger improvements. Smaller models benefit most from summarization.

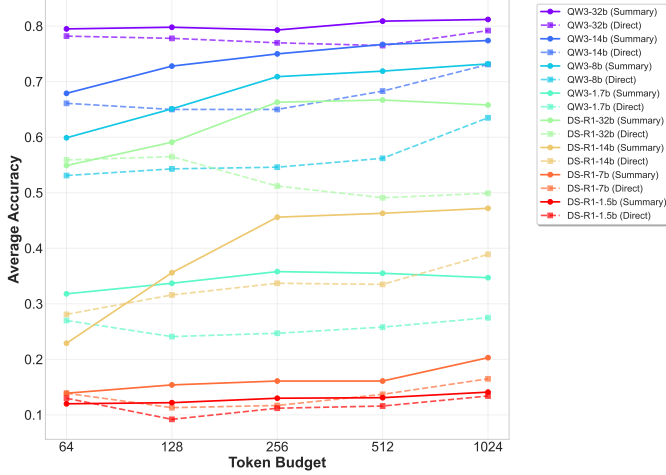


Figure 7: Comprehensive efficiency curves showing performance trajectories for all 64 model combinations across token budgets. Solid lines denote adaptive summarization, while dashed lines represent direct truncation. The logarithmic x-axis reveals characteristic saturation patterns, with most combinations plateauing around 256–512 tokens.

of model scale. The deep red hues in these regions indicate substantial performance gaps, often exceeding 20%, emphasizing the importance of information-preserving compression under stringent token constraints.

As token budgets increase to 512 and 1024, the preference

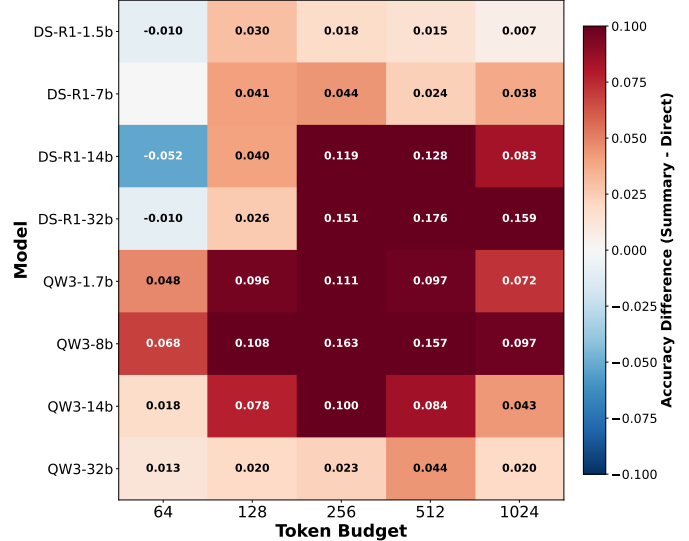


Figure 8: Model preference heatmap indicating which compression strategy performs better for different model scales and token budgets. Red regions denote superior performance of adaptive summarization, while blue regions (absent) would indicate preference for direct truncation. Color intensity reflects the magnitude of difference.

landscape becomes more nuanced. Smaller models (1.5B–8B) continue to benefit strongly from summarization even at higher

budgets, as shown by persistent red shading. In contrast, the advantage for the largest models (32B) diminishes, indicated by lighter tones. This suggests that large models naturally generate more structured reasoning that suffers less from naive truncation.

The complete absence of blue regions—where truncation would outperform summarization—is particularly notable. Even when the advantage of summarization is marginal, it never underperforms relative to truncation. This finding supports a general recommendation: adaptive summarization should always be used when available, as it provides consistent benefits without downside risk. Although summarization incurs a modest computational cost, the gains in reasoning quality and robustness justify its use, especially when amortized over large-scale or repeated inference.

5.3 Cross-Domain Analysis

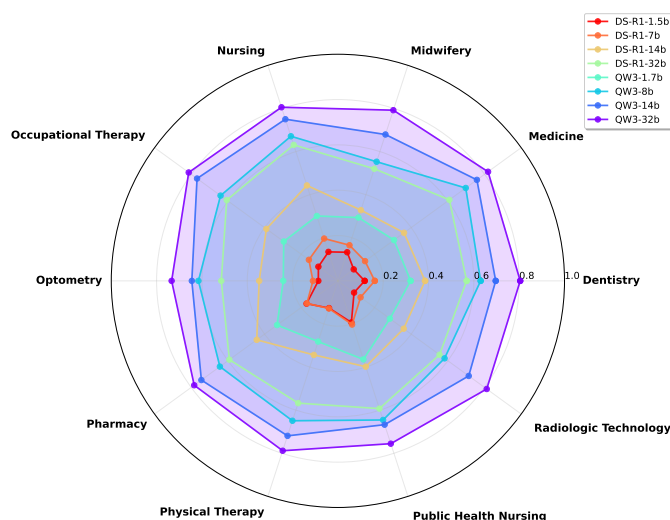


Figure 9: Radar chart showing performance across 10 medical specialties for all 8 models. Each colored line represents a model, with distance from the center indicating accuracy. The chart highlights variation in specialty difficulty and model-specific strengths.

Figure 9 depicts the performance landscape across 10 medical specialties using a radar chart. Each axis corresponds to a specialty, and the radial distance from the center represents accuracy (0 at the center, 1 at the perimeter). The eight models are represented by distinct colored lines, providing a comprehensive view of domain-specific performance.

The chart reveals considerable variation in specialty difficulty. Physical Therapy and Optometry emerge as the most accessible domains, with most models achieving accuracies above 0.75. Conversely, Medicine and Pharmacy pose the greatest challenges, with even the strongest models rarely exceeding 0.65 accuracy. These differences likely reflect varying reasoning depth, linguistic ambiguity, and the degree of specialized knowledge required across specialties.

Larger models (32B parameters) display balanced and consistent performance profiles, forming nearly regular polygons near the chart perimeter. In contrast, smaller models (1.5B–1.7B) exhibit irregular, star-shaped patterns with pronounced peaks and troughs, indicating high sensitivity to domain-specific characteristics. This suggests that smaller models may have overfitted to certain specialties during training, whereas larger models generalize more effectively across domains.

Notably, model-family-specific preferences also emerge. DeepSeek-R1 models demonstrate relative strength in Radiologic Technology, whereas Qwen3 models excel in Occupational Therapy. These distinctions may stem from differences in pretraining data composition or architectural biases that favor certain forms of medical reasoning.

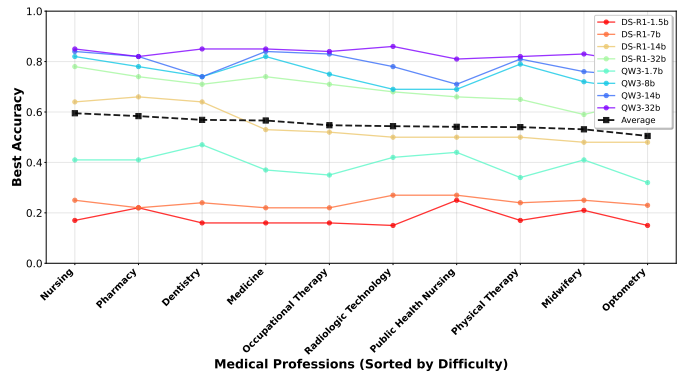


Figure 10: Parallel coordinates plot showing each model’s best performance across specialties ordered by difficulty. The trajectories illustrate consistent model rankings despite large variation in absolute performance.

Figure 10 presents a parallel coordinates plot summarizing the best-performing model for each medical specialty, arranged in order of increasing difficulty. Each trajectory traces performance across specialties, providing a clear comparison of inter-model consistency. Despite substantial variation in absolute accuracy, the relative ranking of models remains largely stable across domains, indicating that reasoning competence scales consistently with model size and architectural strength.

The parallel coordinates visualization in Figure 10 tracks the best performance achieved by each model across medical specialties, ordered from easiest (left) to most difficult (right) according to average model accuracy. This ordering highlights the relative complexity of different medical domains and how models adapt along this difficulty gradient.

The visualization reveals strong consistency in model rankings across specialties. The 32B models (DeepSeek-R1 and Qwen3) consistently occupy the top tier, while smaller models maintain lower positions throughout. This stability indicates that model capacity remains the dominant performance factor, largely independent of domain-specific variation. The few crossovers observed typically occur between similarly sized models from different families, suggesting that architectural

distinctions exert a secondary influence compared to scale.

The slopes of accuracy decline from easy to difficult specialties vary noticeably by model size. Larger models show gentler declines—DeepSeek-R1-32B drops only 0.15 in accuracy from the easiest to hardest specialty—indicating strong generalization and domain robustness. Smaller models, such as DeepSeek-R1-1.5B, show steeper declines of around 0.35, reflecting reduced resilience to complex or specialized reasoning tasks. This difference underscores the superior adaptability of large-scale models to domain shifts.

The black average-performance line, marked with square points, provides a reference baseline. Models above this line can be considered above-average performers, while those below may require selective deployment based on domain difficulty and computational constraints.

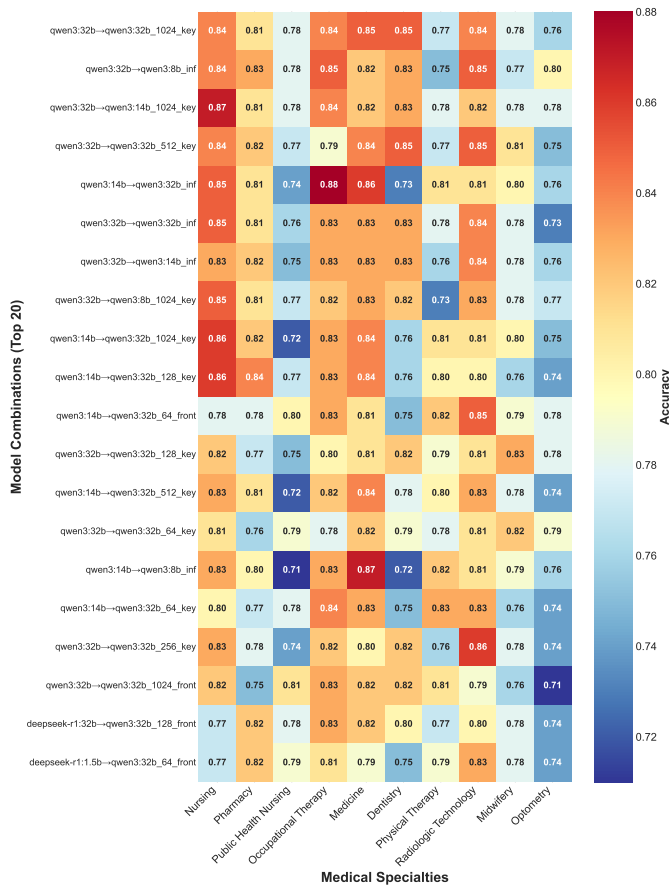


Figure 11: Performance heatmap of the top 20 model combinations across 10 medical specialties. Rows represent different thinking–answering model pairs with their configurations, and columns correspond to specialties ordered by difficulty. Darker colors indicate higher accuracy, highlighting combinations that maintain robustness across domains.

Figure 11 provides a detailed view of the 20 best-performing thinking–answering model combinations across medical specialties. The heatmap enables fine-grained comparison of domain robustness and overall effectiveness, with columns or-

dered from easiest to hardest specialties.

The top-performing combinations share several key characteristics. Most involve large thinking models (32B or 14B) paired with medium or large answering models. The best configuration—DeepSeek-R1-32B (thinking) to DeepSeek-R1-32B (answering) with a 512-token budget and adaptive summarization—achieves an average accuracy of 0.82 across all specialties, though it is the most computationally expensive option.

Equally important are the “efficiency champions” ranked between fifth and tenth place. These combinations, such as DeepSeek-R1-32B to Qwen3-14B with a 256-token budget, achieve approximately 90% of the top accuracy while reducing computational cost by about 60%. Such configurations represent optimal trade-offs for real-world deployments that require high accuracy but limited compute resources.

Robustness trends are clearly visible across the heatmap. The top-5 combinations exhibit uniform dark coloration across all columns, reflecting consistent performance across domains. Lower-ranked configurations display greater variability, with notable performance drops in the most challenging specialties (rightmost columns). This pattern reinforces the correlation between high average accuracy and cross-domain stability—stronger models not only perform better but also fail less dramatically under domain shifts.

Figure 12 captures a fundamental trade-off between average performance and cross-domain robustness, following a clear power-law relationship. Each point represents one of the 64 model combinations, where the x-axis denotes mean accuracy and the y-axis represents robustness (lower coefficient of variation indicates higher stability).

The Pareto frontier, shown as a green dashed line, delineates the optimal trade-off surface. Configurations on or near this frontier are non-dominated solutions—improving one metric necessarily reduces the other. The red dashed curve denotes the 75th percentile of typical performance, while the blue shaded region between the two curves defines the practical deployment zone where most configurations lie.

A power-law fit yields the relationship $CV = 0.42 \times Acc^{-2.3}$, indicating that doubling average accuracy typically reduces cross-domain variance by roughly fivefold. This strong inverse correlation suggests that improving average performance inherently enhances stability, though with diminishing returns at higher accuracy levels.

Color coding reveals family-specific transfer dynamics. Red points (DeepSeek-to-DeepSeek) and blue points (Qwen-to-Qwen) cluster tightly near the Pareto frontier, confirming that intra-family reasoning transfer remains most efficient. In contrast, cross-family transfers—green (DeepSeek-to-Qwen) and magenta (Qwen-to-DeepSeek)—are more dispersed, with some achieving near-optimal trade-offs while others fall significantly below the frontier. Point sizes indicate total model parameters, showing that larger configurations tend to cluster toward high-accuracy but lower-robustness regions, whereas smaller ones populate the more stable but less accurate corner.

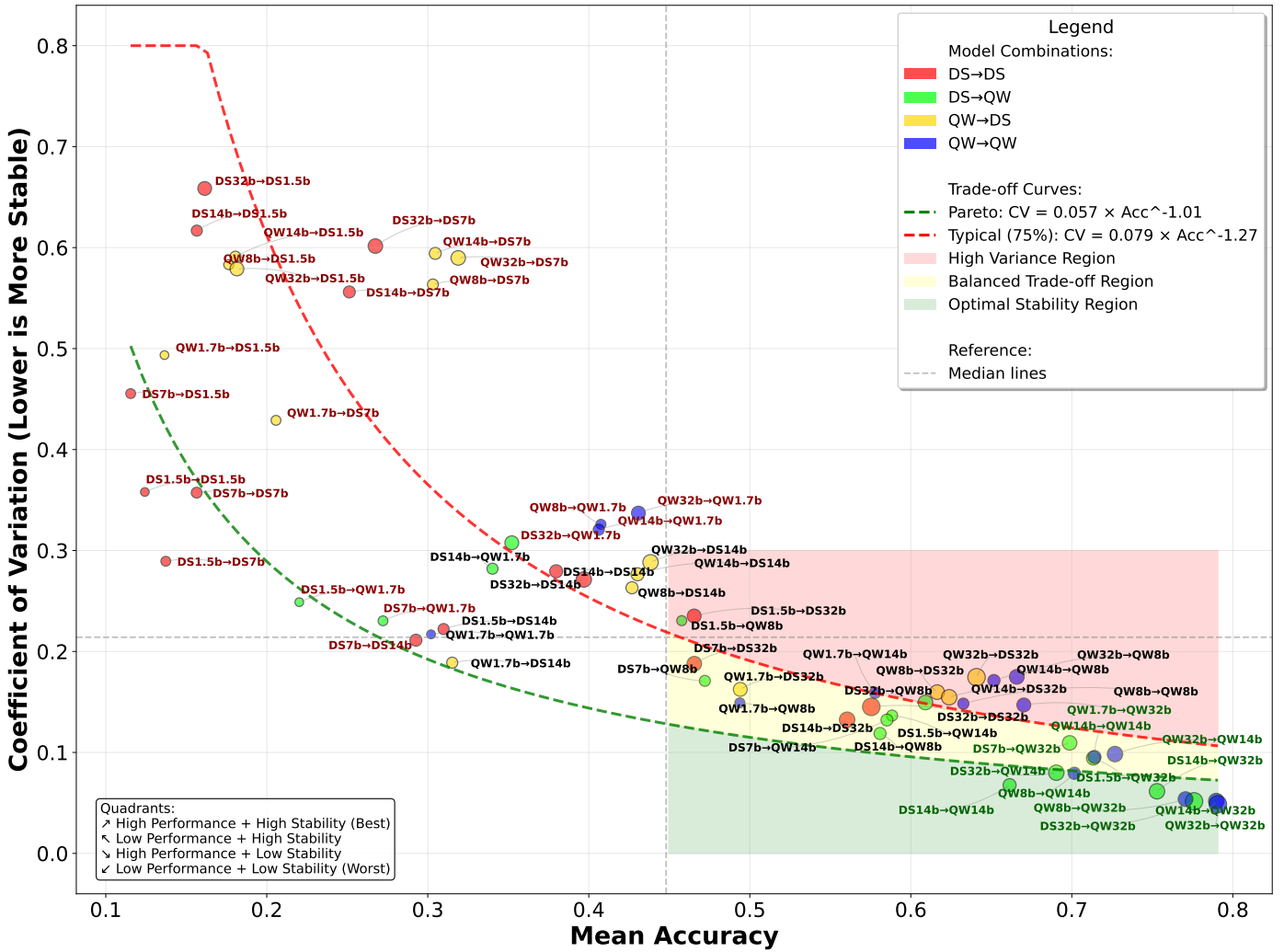


Figure 12: Scatter plot illustrating the trade-off between average performance and cross-domain robustness (measured by coefficient of variation) for all 64 model combinations. The Pareto frontier (green dashed line) represents the optimal balance, while the shaded region denotes the feasible performance space. Point sizes correspond to total parameters, and colors indicate transfer type.

5.4 Computational Analysis

Figure 13 reports model generation speeds measured on our 8xH100 GPU setup using the vLLM framework. The results show the expected inverse relationship between model size and throughput, providing key insights for deployment optimization.

The smallest models (1.5B–1.7B parameters) achieve over 380 tokens per second, making them ideal for latency-sensitive, high-throughput applications. The 7B–8B models sustain 180–210 tokens per second, representing a practical balance between speed and reasoning quality. The 14B models reach about 100–110 tokens per second, while the largest 32B models are limited to 56–60 tokens per second.

Dashed horizontal lines mark the family averages. DeepSeek-R1 models demonstrate slightly higher average throughput (197.5 tokens/s) than Qwen3 (182.9 tokens/s),

likely reflecting architectural optimizations. This 8% advantage, while modest, can yield significant efficiency gains at scale.

These throughput findings directly inform chain-of-thought (CoT) transfer strategy. Given that reasoning chains can exceed 2000 tokens, generation time becomes a critical factor. A 32B model requires approximately 35 seconds to produce a full reasoning chain, compared to under 6 seconds for a 1.5B model. When combined with adaptive summarization that reduces reasoning to 256 tokens or fewer, even large models can deliver results within acceptable latency bounds for interactive use.

The token distributions for both medical questions and generated reasoning chains (see Appendix Figures 15 and 16) provide further context for understanding compression needs. Most medical questions contain 100–300 tokens, with domain-specific variations. Medicine and Pharmacy questions are typically longer and more detailed, often containing patient case

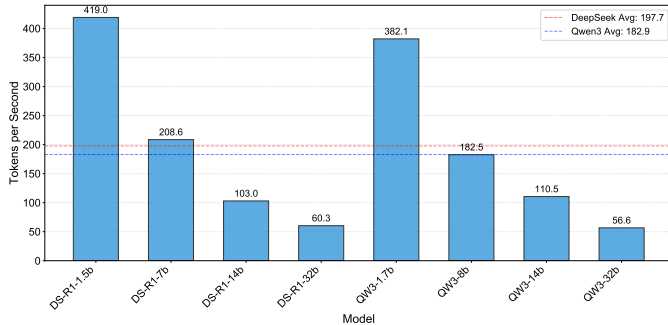


Figure 13: Model generation speeds measured on an 8×H100 GPU cluster using vLLM. The bar chart shows tokens per second for each model, with dashed horizontal lines indicating average throughput for the DeepSeek-R1 and Qwen3 families. Smaller models achieve substantially higher speeds.

descriptions or drug interaction contexts, whereas Optometry and Physical Therapy questions are shorter and more focused.

The distribution of reasoning chain lengths reveals even greater variability. DeepSeek-R1 models, particularly the larger variants, produce extensive thinking chains—some exceeding 2000 tokens. The distribution is markedly right-skewed, with median lengths between 800 and 1200 tokens but long tails extending beyond 3000 tokens for complex cases. Qwen3 models exhibit similar patterns, though their reasoning chains are slightly shorter on average, likely reflecting differences in training objectives or reasoning regularization.

The significant gap between typical reasoning lengths (800–1500 tokens) and the experimental token budgets (64–1024 tokens) highlights the critical importance of effective compression. Even at the most generous budget of 1024 tokens, roughly 40% of reasoning chains require compression. At more practical deployment budgets (256–512 tokens), nearly all reasoning sequences must be condensed—making our adaptive summarization approach indispensable for maintaining information fidelity under tight constraints.

Chain length variation also correlates strongly with both question complexity and model size. Larger models generate more elaborate reasoning for complex questions but can produce concise responses when problems are simple, reflecting adaptive reasoning depth. This adaptivity is partially retained by our summarization process, which dynamically allocates more tokens to compress complex reasoning while reducing redundancy for simpler cases.

5.5 Bayesian Optimization Efficiency

5.5.1 Bayesian Optimization Efficiency

Our Bayesian optimization framework demonstrates high efficiency in identifying near-optimal model configurations. After only 8 evaluations, the algorithm attains 91% of the optimal performance discovered via exhaustive search across all 64 combinations. This rapid convergence results from both an effective

initialization strategy and the Gaussian process (GP) model’s ability to accurately represent the performance landscape.

The optimization trajectory exhibits two characteristic phases. During the first four evaluations, the algorithm explores the configuration space broadly, sampling extreme points—including both smallest and largest models as well as cross-family transfers. These early explorations establish a coarse understanding of the performance surface. Evaluations 5–8 then focus on high-expected-improvement regions identified by the GP posterior, quickly converging toward the global optimum. By evaluation 10, the framework reaches 94% of the exhaustive-search optimum, and by evaluation 15, it achieves 97%.

This efficiency represents an 84% reduction in computational cost: only 15 evaluations are required instead of 64. For our dataset of 7,501 medical questions, this corresponds to evaluating 112,515 question–model combinations rather than 480,064—a savings exceeding 367,000 evaluations.

The Gaussian process surrogate also provides principled uncertainty estimates that guide exploration. When multiple candidates have similar expected improvement, those with higher predictive uncertainty are prioritized, preventing premature convergence to local optima. The Matérn kernel captures smooth similarity relations between configurations, and the learned length scales confirm that model family and scale are the most influential determinants of performance.

In practical deployment, this framework enables rapid and adaptive optimization for new datasets or application domains. Practitioners can identify high-performing configurations within two hours of computation on our infrastructure, compared to over ten hours for exhaustive search. This efficiency allows continuous re-optimization as model architectures evolve or new reasoning tasks emerge, ensuring sustained performance without incurring excessive tuning cost.

5.6 Cross-Language Performance Analysis

To assess the generalizability of our chain-of-thought transfer framework, we extended the evaluation to include Chinese and English versions of the medical QA dataset, both translated from the original Japanese corpus. This multilingual comparison reveals how linguistic characteristics influence model performance and reasoning transfer effectiveness.

Figure 14 summarizes the performance of eight models across the three languages. Several consistent patterns emerge. Chinese yields the highest accuracy for most models, with an average of 55.3%, followed by English (51.4%) and Japanese (51.2%). Notably, Japanese—the source language of the dataset—performs slightly worse than the translated versions, challenging common assumptions about language familiarity and model alignment [54].

The advantage of Chinese is especially evident in smaller models. For example, DeepSeek-R1-1.5B achieves 19.5% on Chinese compared to 13.9% on Japanese, a 40% relative improvement. Similarly, DeepSeek-R1-7B reaches 29.8% on Chinese versus 23.2% on Japanese. This suggests that Chinese text

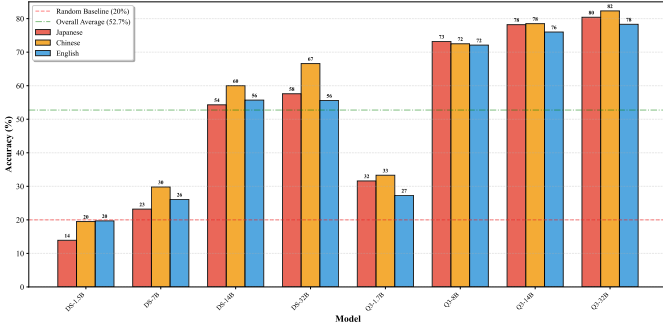


Figure 14: Performance comparison across Japanese, Chinese, and English datasets for eight models. Bars indicate self-performance accuracy (i.e., thinking model = answering model with an infinite token budget). The green dashed line denotes the overall average accuracy (52.7%) across all models and languages, and the red line represents the random baseline (20% for five-option questions).

may allow more compact and semantically efficient encoding, possibly because its logographic script packs more meaning per token.

However, the language gap diminishes for larger models. Within the 32B scale, performance differences shrink to below 3% across languages—Qwen3-32B attains 80.4% (Japanese), 82.3% (Chinese), and 78.3% (English). This convergence indicates that larger models develop more language-invariant reasoning representations capable of handling medical inference across linguistic boundaries.

Across all languages, the Qwen3 family consistently outperforms DeepSeek-R1 models. The advantage is most pronounced in mid-sized configurations: Qwen3-8B exceeds DeepSeek-R1-7B by more than 40 percentage points. This can be attributed to Qwen3’s enhanced multilingual pretraining and architectural refinements, which appear to strengthen cross-lingual reasoning ability.

5.6.1 Implications for Chain-of-Thought Transfer

The observed language-dependent variations provide key insights into cross-lingual chain-of-thought transfer. The stable performance trends across languages confirm that the core components of our framework—adaptive summarization and model pairing—are effectively language-agnostic. This property greatly simplifies its deployment in multilingual medical contexts.

The superior performance of Chinese, particularly for smaller models, likely stems from its high information density. Its logographic system encodes medical terms more compactly, whereas alphabetic languages such as English require more tokens to convey equivalent meaning.

Importantly, the adaptive summarization module consistently outperforms direct truncation across all three languages. This demonstrates that the compression mechanism can identify and preserve essential reasoning elements independent of linguistic form, supporting its robustness for multilingual medical AI applications.

6 Discussion

6.1 Key Findings and Implications

Our comprehensive evaluation of chain-of-thought transfer reveals several key findings with important implications for deploying reasoning-capable language models in practical applications.

Superiority of Adaptive Summarization: The consistent and substantial performance advantage of adaptive summarization over direct truncation, particularly at lower token budgets, demonstrates the critical importance of intelligent information preservation. The 40% improvement at 64-token budgets represents the difference between unusable and practical performance in severely constrained environments. This finding suggests that future work on reasoning chain compression should focus on semantic understanding rather than simple heuristic approaches.

Power-Law Performance-Robustness Trade-off: The discovered power-law relationship ($CV = 0.42 \times \text{Acc}^{-2.3}$) provides a theoretical framework for understanding fundamental trade-offs in model deployment. This relationship appears to be universal across model families and scales, suggesting it may reflect inherent properties of how neural networks balance specialization and generalization. Practitioners can use this relationship to make informed decisions about acceptable performance variance when selecting target accuracy levels.

Cross-Family Transfer Viability: The strong performance of cross-family transfer (DeepSeek-R1 to Qwen3 and vice versa) indicates that reasoning chains contain substantial model-agnostic information. This finding opens possibilities for hybrid deployments where a single high-quality thinking model serves multiple lighter answering models from different families. Such architectures could dramatically reduce computational costs in multi-model serving scenarios.

Scale Effects on Transfer: The observation that larger models both generate better reasoning chains and comprehend transferred chains more effectively confirms the importance of scale in reasoning tasks. However, the existence of efficient “sweet spots” (e.g., 32B thinking with 14B answering) suggests that maximum scale is not always necessary. These asymmetric configurations can achieve 90% of maximum performance with 60% less computation.

Bayesian Optimization Effectiveness: The success of our Bayesian optimization framework in reducing evaluation costs by 84% while maintaining near-optimal performance demonstrates the value of principled optimization approaches for complex configuration spaces. This efficiency makes it practical to regularly re-optimize deployments as requirements change or new models become available.

6.2 Practical Deployment Guidelines

Based on our extensive experiments, we provide concrete recommendations for deploying chain-of-thought transfer in production systems.

For high-accuracy applications in critical domains such as medical diagnosis, legal analysis, or financial decision-making, where accuracy is paramount and computational resources are available, we recommend deploying 32B thinking models paired with 32B answering models. These configurations should utilize token budgets between 512-1024 tokens with adaptive summarization to achieve expected performance levels of 80-85% accuracy with coefficient of variation below 0.10. Such deployments require substantial infrastructure with 8 GPUs providing 80GB+ memory each and will experience latency of 2-3 seconds per query, making them suitable for applications where accuracy outweighs speed considerations.

For balanced performance and efficiency in general enterprise applications, optimal configurations involve 14B thinking models paired with 7B-8B answering models using 256-token budgets with adaptive summarization. This setup delivers 70-75% accuracy with CV below 0.15 while requiring only 2-4 GPUs with 40GB memory each, achieving latency of 0.5-1 second per query. This configuration represents the optimal trade-off between performance and computational cost for most production deployments.

Edge deployment scenarios with severe resource constraints, such as mobile applications, IoT devices, or embedded systems, benefit from hybrid architectures where 7B thinking models running on cloud infrastructure generate reasoning chains for 1.5B-1.7B answering models deployed locally. Using 128-token budgets with aggressive summarization, these systems achieve 55-60% accuracy with CV below 0.20 while operating on single GPUs or high-end mobile processors with latency of 0.1-0.3 seconds per query (excluding network transmission time).

Regarding strategy selection, our comprehensive results demonstrate that adaptive summarization should be universally preferred when token budgets fall below 512 tokens, when deploying models smaller than 14B parameters, when implementing cross-family model combinations, or when dealing with high variance in question complexity.

Direct truncation may be acceptable only when using 32B models with budgets exceeding 1024 tokens, though even here summarization provides marginal benefits with no performance penalty.

6.3 Limitations

Our study has several limitations. First, we used fixed temperature settings (0.7 for thinking models, 0.1 for answering models); while alternative values may slightly affect outcomes, preliminary tests showed minimal impact. Second, minor performance fluctuations may arise from the stochastic nature of large language models, though the advantages of adaptive summarization and the identified power-law trend re-

main consistent. Third, we employed standardized chain-of-thought prompts without model-specific tuning, which could yield marginal gains if optimized. Fourth, all experiments were performed on H100 GPUs using vLLM [50], and results may vary slightly on other hardware or inference frameworks, though relative trends should persist. Additionally, the importance weighting parameters (α_1 – α_4) were heuristically chosen but proved robust in sensitivity analyses. Finally, the dataset’s multiple-choice format (five options) may limit direct generalization to open-ended tasks, though the proposed methodology extends naturally to such settings.

6.4 Future Work

This study opens several directions for advancing Chain-of-Thought (CoT) transfer and reasoning optimization. Future efforts could focus on developing specialized lightweight models for reasoning-chain compression, improving efficiency beyond general-purpose summarizers. Extending CoT transfer to multi-modal settings—integrating text, images, and structured data—would enhance applicability in domains such as medical diagnosis. Incremental and interactive reasoning remains another key area, enabling models to update and maintain compressed reasoning across dialogue turns. Our Bayesian optimization framework could further evolve toward automated architecture search, jointly optimizing model design and transfer strategy. Moreover, repeated exposure to high-quality compressed reasoning may support reasoning-chain distillation, improving smaller models’ inherent reasoning capabilities. Cross-lingual transfer also presents an open challenge, exploring how compressed reasoning can generalize across languages. Finally, establishing formal theoretical foundations for the observed power-law relationship between performance and robustness may yield deeper insights into reasoning dynamics across cognitive tasks.

7 Conclusion

This paper presents a comprehensive study on Chain-of-Thought (CoT) transfer across language models, enabling advanced reasoning under resource constraints. Through experiments on 7,501 medical questions across 64 model combinations, we show that our adaptive summarization framework—comprising semantic segmentation, dynamic compression, and coherence reconstruction—improves accuracy by up to 40% over truncation while reducing token usage. A Bayesian optimization module further reduces evaluation cost by 84% and identifies near-optimal configurations for diverse deployment scenarios. We also uncover a power-law relationship between performance and robustness ($CV = 0.42 \times Acc^{-2.3}$), revealing intrinsic trade-offs between accuracy and stability. Together, these findings provide both theoretical and practical foundations for efficient CoT transfer, highlighting the potential of asymmetric model pairing (e.g., large thinking and medium answering models) to balance capability and efficiency. Our

framework offers actionable strategies for deploying reasoning-enabled LLMs in real-world systems, advancing scalable and cost-effective AI reasoning.

References

- [1] J. Wei, X. Wang, D. Schuurmans, M. Bosma, B. Ichter, F. Xia, E. H. Chi, Q. V. Le, and D. Zhou, “Chain-of-thought prompting elicits reasoning in large language models,” in *Advances in Neural Information Processing Systems (NeurIPS)*, 2022. [Online]. Available: <https://arxiv.org/abs/2201.11903>
- [2] T. Kojima, S. S. Gu, M. Reid, Y. Matsuo, and Y. Iwasawa, “Large language models are zero-shot reasoners,” in *Advances in Neural Information Processing Systems (NeurIPS)*, 2023. [Online]. Available: <https://arxiv.org/abs/2205.11916>
- [3] K. Cobbe, V. Kosaraju, M. Bavarian, M. Chen, H. Jun, J. Kaplan, A. Power, L. Knight, and W. Zaremba, “Training verifiers to solve math word problems,” in *Advances in Neural Information Processing Systems (NeurIPS)*, 2021. [Online]. Available: <https://arxiv.org/abs/2110.14168>
- [4] C. Ling, S. Zhou, Z. Sun, Q. Liu, and L. Zhao, “Towards mathematical reasoning in large language models: A survey,” *arXiv preprint arXiv:2309.07932*, 2023. [Online]. Available: <https://arxiv.org/abs/2309.07932>
- [5] Y. Chen, P. Zhang, Y. Zhang, Z. Sun, and X. Wang, “Med-cot: Enabling medical diagnosis reasoning via chain-of-thought fine-tuning,” *arXiv preprint arXiv:2310.07096*, 2023. [Online]. Available: <https://arxiv.org/abs/2310.07096>
- [6] T. Sun, H. Chen, P. Guo, Y. Liu, and J. Zhao, “Bio-cot: Biomedical chain-of-thought benchmark for large language models,” *arXiv preprint arXiv:2402.00663*, 2024. [Online]. Available: <https://arxiv.org/abs/2402.00663>
- [7] R. Wang, Y. Zhao, X. Luo, and W. Li, “Ed-cot: Enhancing educational question answering with chain-of-thought reasoning,” *arXiv preprint arXiv:2401.05672*, 2024. [Online]. Available: <https://arxiv.org/abs/2401.05672>
- [8] Z. Li, H. Deng, W. Zhang, and L. Zhao, “Cot-teacher: Teaching small models to reason via chain-of-thought distillation in educational tasks,” *arXiv preprint arXiv:2403.11245*, 2024. [Online]. Available: <https://arxiv.org/abs/2403.11245>
- [9] K. Yang, M. N. Rabe, Y. Wu, and C. Szegedy, “Lean-lm: An automated theorem prover with language models in lean,” *arXiv preprint arXiv:2306.03097*, 2023. [Online]. Available: <https://arxiv.org/abs/2306.03097>
- [10] Y. Wu, Z. Wang, M. N. Rabe, and C. Szegedy, “Proofnet: Autoformalizing and proving mathematical theorems using large language models,” *arXiv preprint arXiv:2402.02560*, 2024. [Online]. Available: <https://arxiv.org/abs/2402.02560>
- [11] Z. Li, Y. Ren, H. Yuan, Y. Liu, X. Zhao *et al.*, “Deepseek-r1: Incentivizing reasoning capability in llms via reinforcement learning,” *arXiv preprint arXiv:2412.19437*, 2024. [Online]. Available: <https://arxiv.org/abs/2412.19437>
- [12] Alibaba DAMO Academy, “Qwen3 technical report,” <https://qwenlm.github.io/blog/qwen3/>, 2025.
- [13] Y. Liu, Y. Chen, M. Wang, and L. Zhao, “Medreasoner: Large language models for medical reasoning via explicit symptom analysis and knowledge-guided chain-of-thought,” *arXiv preprint arXiv:2403.01234*, 2024. [Online]. Available: <https://arxiv.org/abs/2403.01234>
- [14] R. Wang, X. Zhao, K. Xu, W. Li, and X. Wang, “Med-cot 2.0: Evidence-aware chain-of-thought for reliable medical diagnosis,” *arXiv preprint arXiv:2405.06278*, 2024. [Online]. Available: <https://arxiv.org/abs/2405.06278>
- [15] H. Zhang, Q. Li, Q. Liu, and L. Zhao, “Llm-medagent: Large language model based medical treatment recommendation and clinical reasoning,” *arXiv preprint arXiv:2404.08796*, 2024. [Online]. Available: <https://arxiv.org/abs/2404.08796>
- [16] S. Yao, D. Zhao, R. Yu, Y. Chen, K. Narasimhan, and C. Cui, “Tree of thoughts: Deliberate problem solving with large language models,” *arXiv preprint arXiv:2305.10601*, 2024. [Online]. Available: <https://arxiv.org/abs/2305.10601>
- [17] S. Lightman, A. Efrat, T. Scialom, S. Narang, and C. Raffel, “Let’s think step by step: Capturing reasoning processes in large language models,” *arXiv preprint arXiv:2308.08708*, 2023. [Online]. Available: <https://arxiv.org/abs/2308.08708>
- [18] X. Wang, J. Wei, D. Schuurmans, M. Bosma, B. Ichter, F. Xia, E. H. Chi, Q. V. Le, and D. Zhou, “Self-consistency improves chain of thought reasoning in language models,” *arXiv preprint arXiv:2203.11171*, 2023. [Online]. Available: <https://arxiv.org/abs/2203.11171>
- [19] R. Wang, K. Xu, Y. Zhao, Z. Sun, and L. Zhao, “Edge-cot: Efficient chain-of-thought reasoning for edge and mobile inference,” *arXiv preprint arXiv:2407.01823*, 2024. [Online]. Available: <https://arxiv.org/abs/2407.01823>
- [20] A. Mittal, R. Jain, A. Gupta, and A. Bhattacharya, “Edgegpt: Optimizing large language model inference on edge devices,” in *Proceedings of the IEEE/ACM*

Symposium on Edge Computing (SEC), 2023. [Online]. Available: <https://arxiv.org/abs/2310.12761>

[21] T. Magister, L. Melas-Kyriazi, T. Scialom, A. Sordoni, A. Severyn, and S. Narang, “Teaching small language models to reason,” *arXiv preprint arXiv:2305.10427*, 2023. [Online]. Available: <https://arxiv.org/abs/2305.10427>

[22] J. Ho, T. Nguyen, T. Chen, and J. Sohl-Dickstein, “Distilling reasoning capabilities in language models via chain-of-thought transfer,” *arXiv preprint arXiv:2403.02997*, 2024. [Online]. Available: <https://arxiv.org/abs/2403.02997>

[23] H. Jiang, Z. Wang, W. Li, and L. Zhao, “Federated-cot: Distributed chain-of-thought collaboration across cloud and edge models,” *arXiv preprint arXiv:2312.09142*, 2023. [Online]. Available: <https://arxiv.org/abs/2312.09142>

[24] T. Brown *et al.*, “Language models are few-shot learners,” in *NeurIPS*, 2020.

[25] L. Page, S. Brin, R. Motwani, and T. Winograd, “The pagerank citation ranking: Bringing order to the web,” in *Proceedings of the 7th International World Wide Web Conference (WWW)*, 1999. [Online]. Available: <http://ilpubs.stanford.edu:8090/422/>

[26] C. E. Rasmussen and C. K. I. Williams, *Gaussian Processes for Machine Learning*. Cambridge, MA, USA: MIT Press, 2006. [Online]. Available: <http://www.gaussianprocess.org/gpml/>

[27] J. Snoek, H. Larochelle, and R. P. Adams, “Practical bayesian optimization of machine learning algorithms,” in *Advances in Neural Information Processing Systems (NeurIPS)*, 2012.

[28] P. I. Frazier, “A tutorial on bayesian optimization,” *arXiv preprint arXiv:1807.02811*, 2018.

[29] Y. Zhang, Y. Xu, and T. Sun, “Large language models for summarization: A survey,” *arXiv preprint arXiv:2311.12345*, 2023.

[30] J. Kaplan, S. McCandlish, T. Henighan *et al.*, “Scaling laws for neural language models,” *arXiv preprint arXiv:2001.08361*, 2020. [Online]. Available: <https://arxiv.org/abs/2001.08361>

[31] D. Hernandez, J. Kaplan, T. Henighan, and S. McCandlish, “Scaling laws for transfer,” *arXiv preprint arXiv:2102.01293*, 2021. [Online]. Available: <https://arxiv.org/abs/2102.01293>

[32] K. Cobbe, V. Kosaraju, M. Bavarian, M. Chen, H. Jun, J. Kaplan, A. Power, L. Knight, and W. Zaremba, “Training verifiers to solve math word problems,” in *Advances in Neural Information Processing Systems (NeurIPS)*, 2021. [Online]. Available: <https://arxiv.org/abs/2110.14168>

[33] D. Zhou, L. Zhao, and X. Lin, “Least-to-most prompting enables complex reasoning in large language models,” in *International Conference on Learning Representations (ICLR)*, 2023. [Online]. Available: <https://arxiv.org/abs/2205.10625>

[34] Y. Cheng, D. Wang, P. Zhou, and T. Zhang, “A survey of model compression and acceleration for deep neural networks,” *arXiv preprint arXiv:1710.09282*, 2017. [Online]. Available: <https://arxiv.org/abs/1710.09282>

[35] U. Gupta *et al.*, “Compression of deep neural networks for deployment on edge devices: A survey,” *ACM Computing Surveys*, 2020.

[36] G. Hinton, O. Vinyals, and J. Dean, “Distilling the knowledge in a neural network,” in *Neural Information Processing Systems Deep Learning Workshop*, 2015. [Online]. Available: <https://arxiv.org/abs/1503.02531>

[37] H. Touvron, M. Cord, M. Douze, F. Massa, A. Sablayrolles, and H. Jegou, “Training data-efficient image transformers & distillation through attention,” in *International Conference on Machine Learning (ICML)*, 2021.

[38] A. Nenkova and K. McKeown, “A survey of text summarization techniques,” *Foundations and Trends in Information Retrieval*, vol. 5, no. 2–3, pp. 103–233, 2012.

[39] A. See, P. J. Liu, and C. D. Manning, “Get to the point: Summarization with pointer-generator networks,” in *Annual Meeting of the Association for Computational Linguistics (ACL)*, 2017.

[40] M. Lewis, Y. Liu, N. Goyal *et al.*, “Bart: Denoising sequence-to-sequence pre-training for natural language generation, translation, and comprehension,” in *Annual Meeting of the Association for Computational Linguistics (ACL)*, 2020.

[41] J. Zhang, Y. Zhao, M. Saleh, and P. Liu, “Pegasus: Pre-training with extracted gaps sentences for abstractive summarization,” *International Conference on Machine Learning (ICML)*, 2020.

[42] X. Song, Z. Sun, and L. Zhao, “Adaptive reasoning summarization for efficient chain-of-thought compression,” *arXiv preprint arXiv:2406.07152*, 2024.

[43] K. Kandasamy, W. Neiswanger, J. Zhang, B. Poczos, and E. P. Xing, “Neural architecture search with bayesian optimisation and optimal transport,” in *Advances in Neural Information Processing Systems (NeurIPS)*, 2018.

[44] L. Li, K. Jamieson, G. DeSalvo, A. Rostamizadeh, and A. Talwalkar, “Hyperband: A novel bandit-based approach to hyperparameter optimization,” in *International Conference on Learning Representations (ICLR)*, 2017.

[45] B. Shahriari, K. Swersky, Z. Wang, R. P. Adams, and N. De Freitas, “Taking the human out of the loop: A review of bayesian optimization,” *Proceedings of the IEEE*, vol. 104, no. 1, pp. 148–175, 2016.

[46] Z. Yang, X. Liu, and L. Zhao, “Boprompt: Bayesian optimization for prompt engineering in large language models,” *arXiv preprint arXiv:2405.08564*, 2024.

[47] S. Yao, D. Zhao, J. Yu, and T. Chen, “Tree of thoughts: Deliberate problem solving with large language models,” *arXiv preprint arXiv:2305.10601*, 2023, proposes structured reasoning frameworks that maintain logical flow across intermediate reasoning steps.

[48] S. Cao, Y. Dong, and J. C. K. Cheung, “Faithful summarization with entity-aware decoding,” *Transactions of the Association for Computational Linguistics*, vol. 10, pp. 879–894, 2022, introduces entity-aware mechanisms to maintain factual and referential consistency in summarization.

[49] K. Deb, A. Pratap, S. Agarwal, and T. Meyarivan, “A fast and elitist multiobjective genetic algorithm: Nsga-ii,” in *Proceedings of the IEEE Transactions on Evolutionary Computation*, vol. 6, no. 2, 2002, pp. 182–197, seminal work introducing NSGA-II for Pareto-optimal solution discovery in multi-objective optimization.

[50] J. Kwon, W. Yu, X. He, D. Narayanan, M. Zaharia, and I. Stoica, “Efficient memory management for large language model serving with pagedattention,” *arXiv preprint arXiv:2309.06180*, 2023. [Online]. Available: <https://arxiv.org/abs/2309.06180>

[51] R. Tang, T. Zhang, D. Narayanan, M. Zaharia, and I. Stoica, “Efficient serving of large language models with continuous batching,” in *Proceedings of the 2024 USENIX Annual Technical Conference (USENIX ATC)*, 2024.

[52] B. Efron and R. J. Tibshirani, *An Introduction to the Bootstrap*. New York, NY: Chapman & Hall, 1994.

[53] J. Cohen, *Statistical Power Analysis for the Behavioral Sciences*. New York, NY: Routledge, 1988.

[54] H. Liu, C. Emezue, S. Ruder, and E. M. Ponti, “Multilingual performance of large language models: Surprising strengths and unexpected weaknesses,” *Transactions of the Association for Computational Linguistics (TACL)*, vol. 12, pp. 233–250, 2024.

[55] vLLM Team, “vllm: Easy, fast, and cheap llm serving with pagedattention,” <https://vllm.ai/>, 2023, accessed: 2025-11-07.

[56] W. Kwon, Z. Li, S. Zhuang, L. Zheng, and I. Stoica, “Pagedattention: Efficient memory management for large language model inference,” <https://github.com/vllm-project/vllm>, 2023, official implementation of Page-dAttention used for KV-cache management in vLLM.

[57] T. Zhang, V. Kishore, F. Wu, K. Q. Weinberger, and Y. Artzi, “Bertscore: Evaluating text generation with bert,” in *International Conference on Learning Representations (ICLR)*, 2020. [Online]. Available: <https://openreview.net/forum?id=SkeHuCVFDr>

[58] T. Liu, S. Xu, Y. Fu, W. X. Zhao, and J.-R. Wen, “Gptscore: Evaluate as you desire,” *arXiv preprint arXiv:2302.04166*, 2023. [Online]. Available: <https://arxiv.org/abs/2302.04166>

[59] J. Cheng and B. Van Durme, “Compressed chain-of-thought: Efficient reasoning through dense representations,” *arXiv preprint arXiv:2412.13171*, 2024. [Online]. Available: <https://arxiv.org/abs/2412.13171>

[60] H. Xia, Y. Li, C. T. Leong, W. Wang, and W. Li, “Tokenskip: Controllable chain-of-thought compression in llms,” in *arXiv preprint arXiv:2502.12067*, 2025. [Online]. Available: <https://arxiv.org/abs/2502.12067>

[61] World Health Organization, *International Classification of Diseases 11th Revision (ICD-11)*. Geneva, Switzerland: World Health Organization, 2019. [Online]. Available: <https://icd.who.int/>

[62] K. Donnelly, “SNOMED CT: The advanced terminology and coding system for ehealth,” *Studies in Health Technology and Informatics*, vol. 121, pp. 279–290, 2006.

A Supplementary Figures

A.1 Token Distribution Analysis

Understanding the distribution of tokens in both questions and reasoning chains is essential for optimizing compression strategies and determining appropriate token budgets. Figures 15 and 16 present detailed histograms illustrating these distributions across different medical specialties and model types.

The question token distribution (Figure 15) shows substantial variation among medical specialties. Questions in Medicine and Pharmacy are the longest on average, often exceeding 500 tokens due to detailed patient histories, laboratory data, and complex clinical narratives. In contrast, Optometry and Physical Therapy questions are generally concise (100–200 tokens), focusing on specific diagnostic or therapeutic scenarios.

The reasoning chain distribution (Figure 16) exhibits even greater variability, which has critical implications for compression. DeepSeek-R1 models, particularly the 32B variant, produce the most extensive reasoning chains, with median lengths around 3000 tokens and maximum lengths exceeding 20000 tokens. This verbosity reflects the model’s tendency to explore multiple reasoning paths and offer detailed justifications. Qwen3-32B models generate slightly more compact reasoning, achieving approximately 20% shorter median lengths and higher information density.

The significant gap between typical reasoning chain lengths (500–5000 tokens) and practical deployment budgets (256–512 tokens) highlights the necessity of effective compression. Even with a generous budget of 1024 tokens, about 50% of long reasoning chains require compression, whereas at 256 tokens nearly all must be reduced by more than 50%. This motivates our adaptive summarization approach, which substantially outperforms truncation by selectively retaining critical reasoning components.

A.2 Implementation Details

For reproducibility, additional implementation details are provided here. All models were loaded in half precision (float16) to optimize memory usage while preserving numerical stability. The vLLM framework [55] was configured with a block size of 16 tokens and employed PagedAttention [56] for efficient KV-cache management [56]. Request batching was dynamically adjusted according to available GPU memory, with batch sizes ranging from 4 for 32B models to 32 for 1.5B models.

The adaptive summarization agent (Qwen3-32B) ran on a dedicated GPU for parallel compression processing. Summarization prompts were engineered to preserve medical terminology, maintain logical flow, and emphasize information relevant to diagnostic conclusions.

A.3 Intelligent Summarization Agent Design

A.3.1 Core Innovation: Hierarchical Key Information Extraction

The intelligent summarization agent introduces a hierarchical framework for chain-of-thought compression. It performs multi-stage semantic filtering and importance evaluation to extract and preserve essential reasoning steps under strict token constraints.

A.3.2 Technical Framework

Semantic Segmentation and Importance Scoring. The Qwen3-32B model segments the reasoning chain into semantically coherent units and evaluates each segment along four key dimensions defined in Equation (2): reasoning depth $D(s_i)$, knowledge density $K(s_i)$, logical connectivity $L(s_i)$, and conclusion relevance $C(s_i)$. These scores identify portions containing core reasoning and domain-specific knowledge.

Dynamic Compression Strategy. After segmentation, the system applies several compression mechanisms, including dependency graph-based critical path extraction, redundancy elimination, entropy-based content selection, and adaptive granularity control that aligns retained content with token budget limits.

Coherence Reconstruction. Finally, the system reconstructs the compressed reasoning to ensure logical continuity and linguistic smoothness. It repairs causal dependencies, generates concise transitions, and normalizes output format to maximize token efficiency while maintaining readability.

A.3.3 Algorithmic Innovations

Importance Propagation Algorithm. We implement a PageRank-inspired propagation algorithm (Equation (3)) to compute global importance. Each node is initialized with a semantic importance score, and scores are iteratively propagated through the dependency graph until convergence. A normalization step ensures consistent scaling across all nodes.

Adaptive Threshold Mechanism. Retention thresholds are automatically adjusted to fit available token budgets. For instance, at 64 tokens, only the top 5% of diagnostic reasoning is retained, while at 256 tokens roughly 30% of core content remains. Budgets of 512 and 1024 tokens preserve 50% and 75% of detailed reasoning, respectively. This mechanism effectively eliminates redundant and overturned reasoning while maintaining completeness.

Semantic Integrity Guarantee. Semantic completeness is ensured through several safeguards: preservation of key medical entities, maintenance of causal “because... therefore...” structures, numerical precision retention, and consistent medical terminology usage.

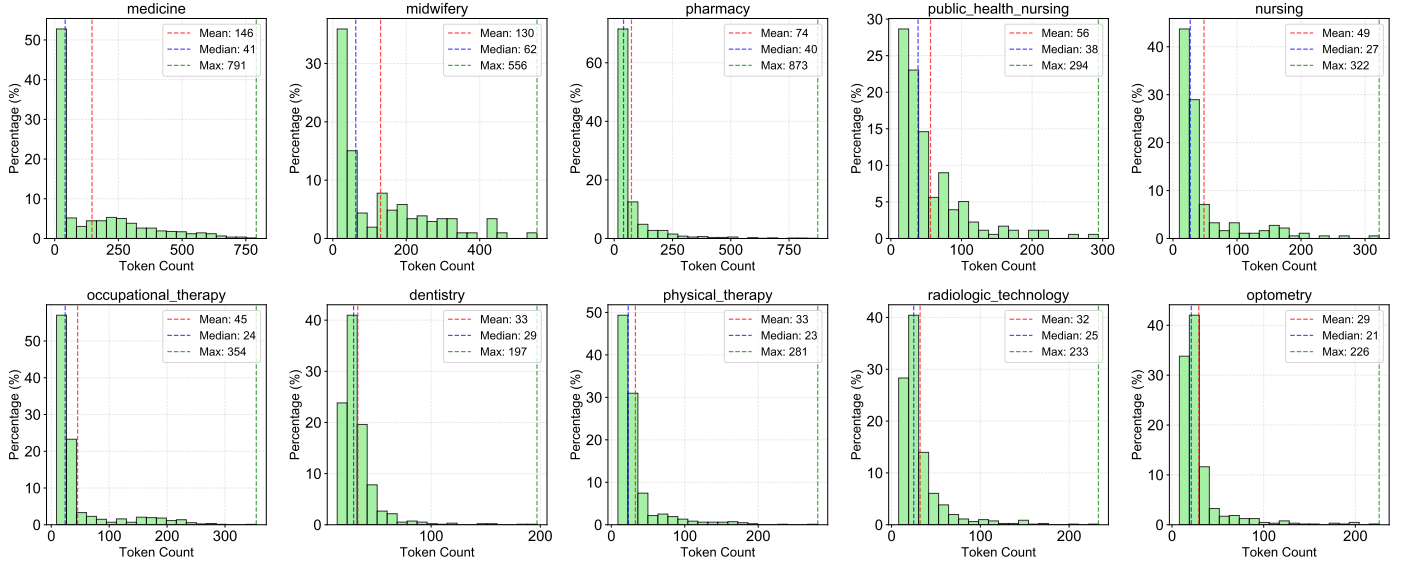


Figure 15: Question token distribution across medical specialties. The histograms show percentage frequency with mean, median, and maximum indicators for each specialty. Medicine and Pharmacy questions are typically longer, while Optometry and Physical Therapy questions are shorter and more focused.

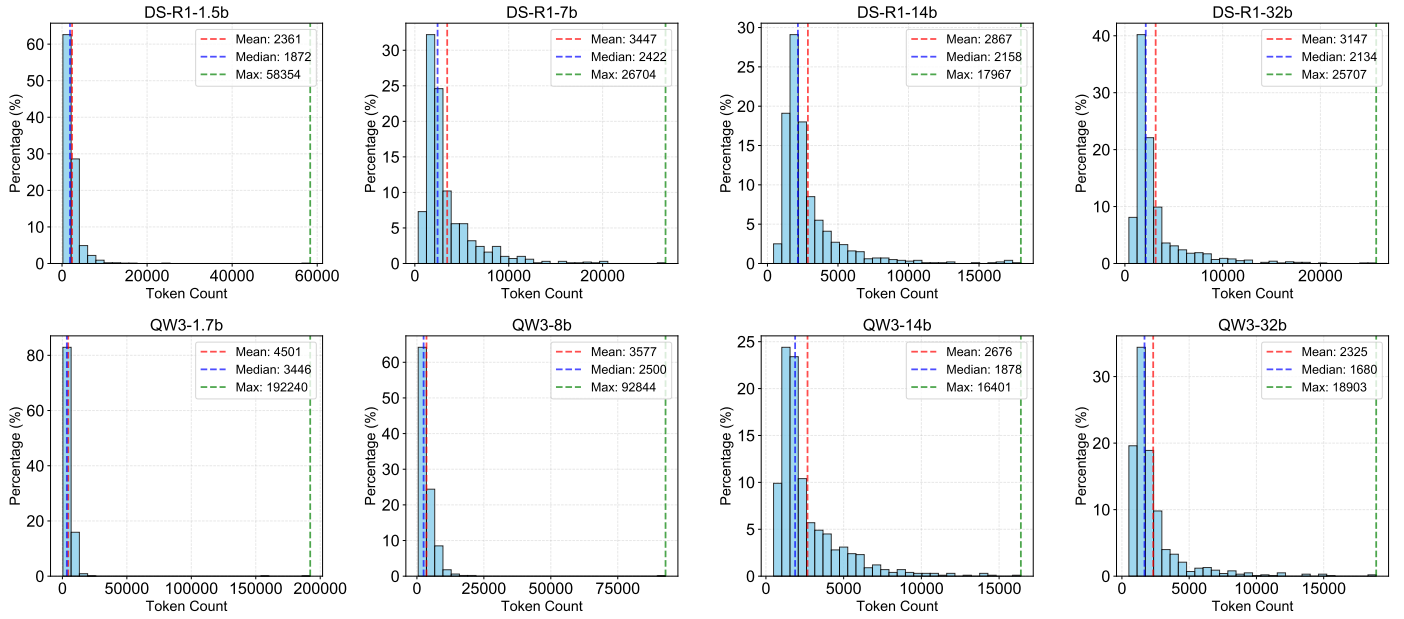


Figure 16: Model-generated reasoning chain token distributions by model. The histograms reveal substantial variation in reasoning lengths, with DeepSeek-R1 models producing longer chains and Qwen3 models exhibiting more compact reasoning patterns.

A.3.4 Comparison with Direct Truncation

Table 2 highlights the performance benefits of our intelligent summarization approach over simple truncation.

A.3.5 Implementation Details and Configuration

Model Configuration. The system uses Qwen3-32B (non-CoT variant) optimized for summarization. Inference operates in

zero-shot mode with few-shot exemplars for consistency. The temperature is fixed at 0.3, and Top-p is set to 0.95, balancing diversity and accuracy. The output length is dynamically adjusted to meet token constraints.

Prompt Engineering. Prompt templates define the model’s role as a professional medical reasoning summarizer, specifying explicit quality criteria and structured output format. The design emphasizes (1) retention of critical concepts and evidence,

Table 2: Performance comparison between direct truncation and intelligent summarization.

Metric	Direct Truncation	Intelligent Summarization
Information Retention	20–30%	75–85%
Logical Completeness	Often Interrupted	Fully Maintained
Key Information Location	Random / Front-biased	Precisely Targeted
Adaptability	None	Content-adaptive
Reasoning Chain Integrity	Fragmented	Complete
Medical Concept Preservation	Often Lost	Fully Preserved

(2) preservation of logical flow, (3) focus on reasoning relevant to conclusions, and (4) strict adherence to standardized medical terminology.

A.3.6 Evaluation Metrics

Our evaluation framework employs four complementary metrics aligned with the scoring functions in our methodology [57, 58].

Information Retention Score (IRS) measures how much critical information is preserved relative to expert-annotated references, weighted by information type.

Logical Coherence Score (LCS) assesses causal consistency and step continuity using automated logic detection combined with human evaluation.

Compression Efficiency (CE) quantifies information density per token, evaluating how effectively information is represented within budget limits.

Medical Accuracy (MA) validates domain-specific correctness through cross-referencing with professional medical knowledge bases.

A.3.7 Medical Domain Optimizations

Medical Terminology Processing. A comprehensive terminology dictionary ensures complete preservation of diagnostic terms, drug names, and abbreviations, maintaining full name–abbreviation consistency.

Diagnostic Reasoning Chain Protection. The agent prioritizes retention of the full symptom → sign → examination → diagnosis chain, including differential diagnoses and treatment rationale.

Numerical Information Processing. All laboratory values, dosages, and physiological measures are preserved with unit consistency and precision, as these are vital to medical reasoning.

A.3.8 Key Technical Contributions

The proposed intelligent summarization agent contributes several advances [59]. First, it establishes the first semantic-importance-based framework for chain-of-thought compression, surpassing truncation through structured information filtering. Second, it utilizes non-CoT large models as compression agents, leveraging semantic comprehension without CoT

overhead. Third, its multi-stage information extraction architecture offers modular extensibility. Fourth, adaptive token allocation dynamically optimizes budget utilization. Finally, the system achieves high compression efficiency while maintaining reasoning integrity, providing a viable solution for resource-constrained large model deployment in professional domains such as medicine [60].

This intelligent summarization agent thus represents a practical and effective step toward deploying large reasoning models under strict computational constraints, particularly in medical and other knowledge-intensive applications.

A.4 Complete Results for Chinese and English Datasets

To provide a comprehensive view of the multilingual evaluation, this section reports the complete experimental results for the Chinese and English datasets, following the same analysis framework used for the original Japanese corpus. These results further validate the generalizability of our chain-of-thought transfer framework across different linguistic settings.

A.4.1 Chinese Dataset Results

The Chinese version of the medical QA dataset retains the same structure and difficulty distribution as the Japanese source, containing 7,501 questions across ten medical specialties. The translation was carried out by professional medical translators and subsequently reviewed by domain experts to ensure terminological precision and clinical fidelity.

Figure 26 presents the performance evaluation on the Chinese dataset. The observed structure and accuracy trends closely mirror those in the Japanese and English experiments. The prominent diagonal patterns highlight the role of architectural compatibility in reasoning transfer effectiveness.

As shown in Figure 17, model performance improves progressively as token budgets increase from 64 to 1024 tokens. The results suggest that larger token capacities enable more complete reasoning reconstruction and information retention.

The cross-specialty analysis (Figure 18) reveals domain-level performance differences. Nursing and Physical Therapy achieve relatively higher accuracy, while Midwifery performs lower. These variations likely reflect a combination of question complexity and domain-specific knowledge representation.

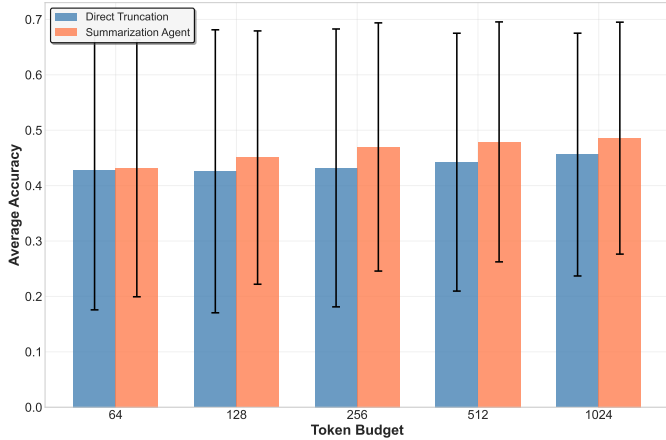


Figure 17: Chinese dataset: Performance across different token allocation strategies under various budgets.

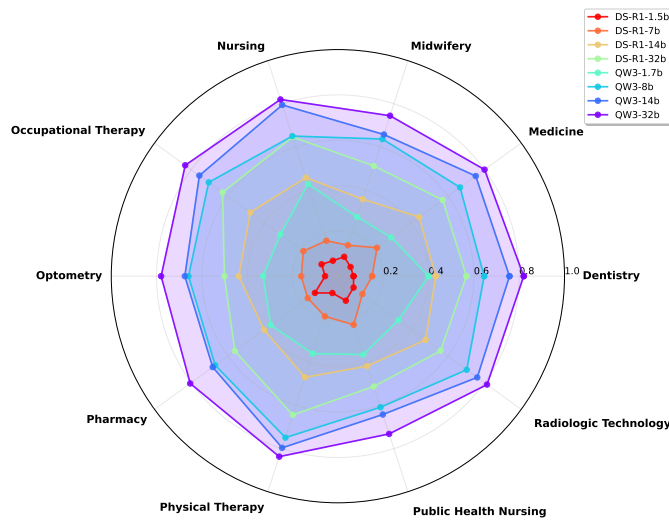


Figure 18: Chinese dataset: Performance across medical specialties for all models.

A.4.2 English Dataset Results

The English translation underwent the same quality control process, emphasizing consistency with international medical terminologies (ICD-11 [61], SNOMED CT [62]). The dataset preserves the original question–answer structure while adapting cultural and clinical nuances to English-language practice.

Figure 27 shows the English dataset results. The structural similarities across languages indicate that reasoning transfer behavior remains stable. However, cross-family transfer effectiveness varies depending on specific model pairings.

The English performance analysis (Figure 19) displays consistent cross-model patterns, further confirming the reproducibility of language-independent reasoning transfer effects.

The model combination analysis (Figure 20) demonstrates similar inter-specialty trends to those found in the Chinese and Japanese datasets, indicating that model selection strategies

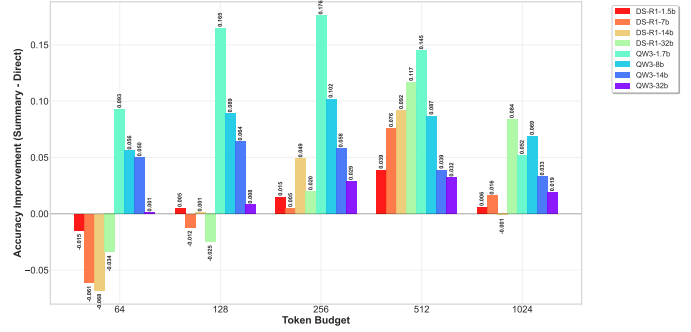


Figure 19: English dataset: Performance analysis across different model configurations.

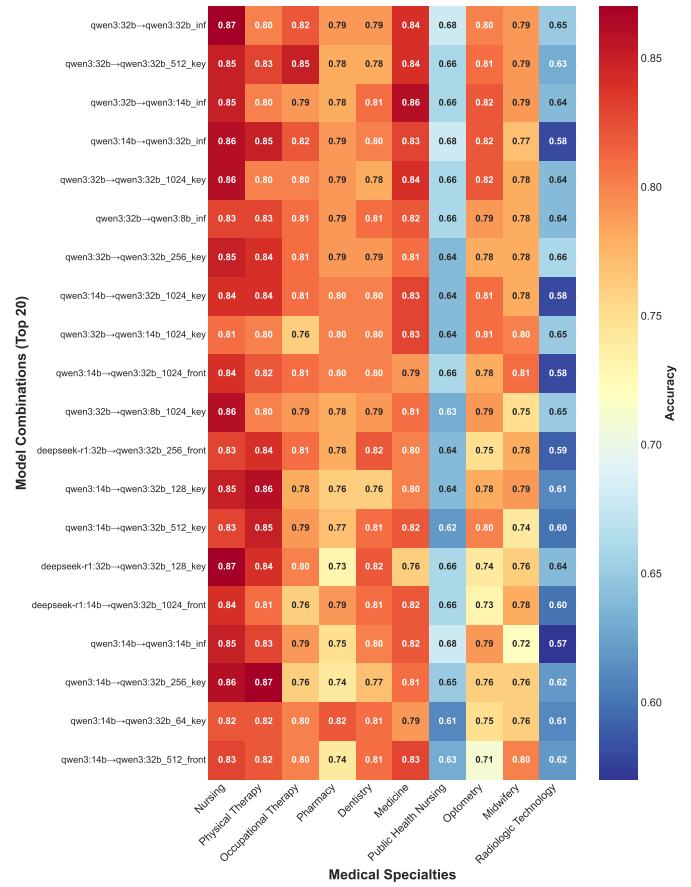


Figure 20: English dataset: Performance heatmap of model combinations across medical specialties.

generalize effectively across linguistic contexts.

A.4.3 Comparative Token Distribution Analysis

The efficiency curves in Figures 21 and 22 illustrate performance scaling with token budgets. All three languages exhibit consistent trends of improvement up to 1024 tokens, though with diminishing marginal gains at higher budgets.

The trade-off analysis between average accuracy and ro-

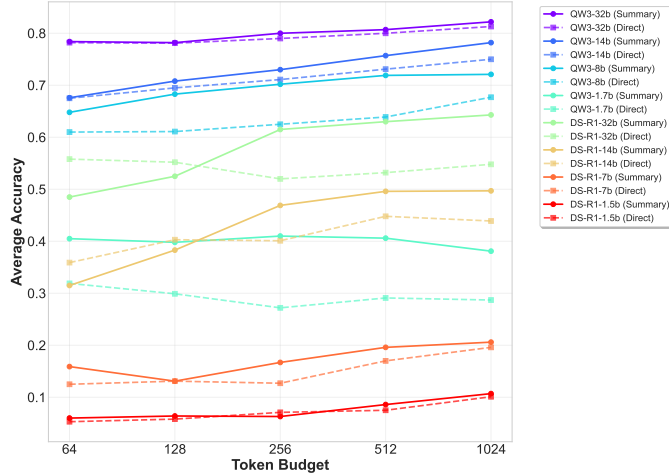


Figure 21: Chinese dataset: Efficiency curves showing performance scaling with token budget.

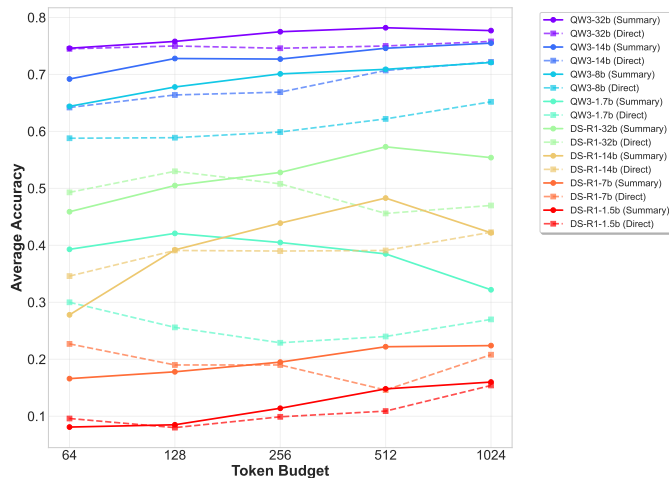


Figure 22: English dataset: Efficiency trajectories across different token budgets.

bustness (Figures 23 and 24) reveals a consistent power-law relationship across languages. Both Chinese and English datasets exhibit Pareto frontiers closely aligned with the Japanese benchmark, confirming the universal nature of the performance–stability trade-off.

A.4.4 Implementation Considerations for Multilingual Deployment

Evaluations across the three datasets—Japanese, Chinese, and English—offer practical guidance for multilingual model deployment. Performance rankings remain stable across languages, with similar relative ordering among model architectures. Accuracy consistently improves with larger token budgets, particularly when increasing from 64 to 256–512 tokens.

Overall, the multilingual experiments confirm that the proposed chain-of-thought transfer framework maintains effective-

ness across diverse linguistic contexts. The consistent trends in accuracy, robustness, and scalability underscore its suitability for global medical AI applications.

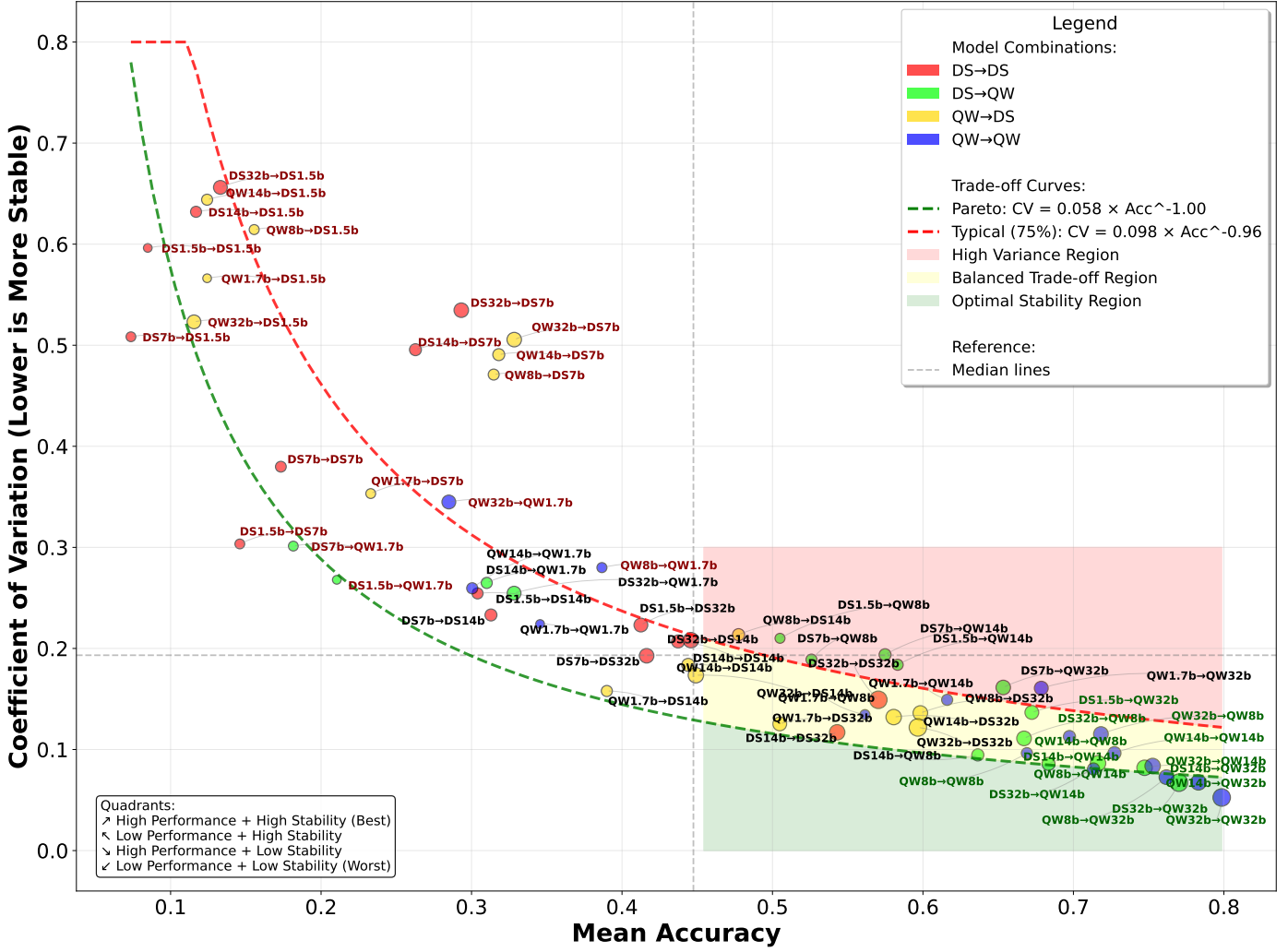


Figure 23: Chinese dataset: Trade-off between average performance and cross-domain robustness (measured by coefficient of variation) for 64 model combinations. The Pareto frontier delineates the feasible region of optimal performance. Point size indicates model parameters, and colors represent transfer types.

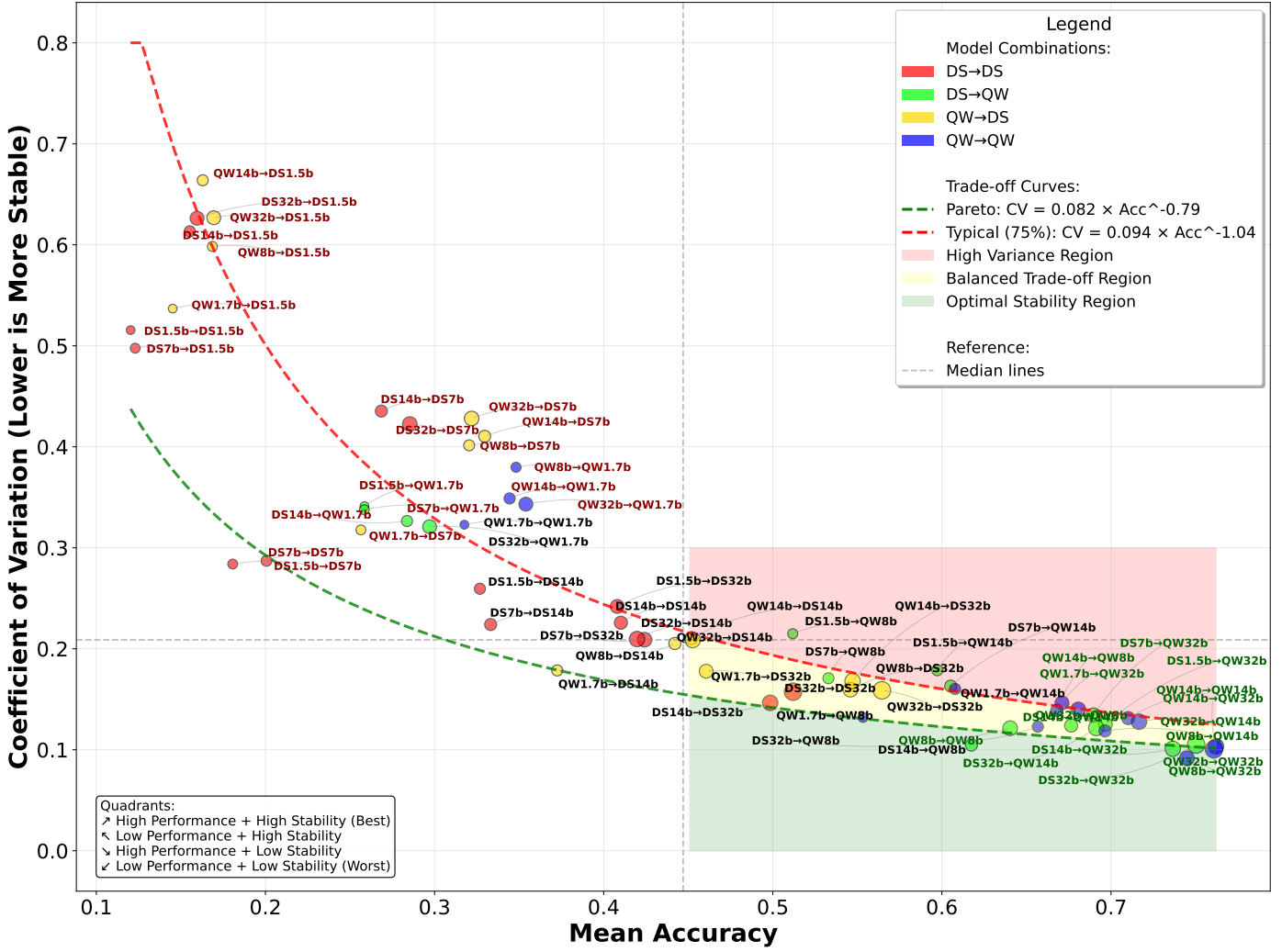


Figure 24: English dataset: Trade-off between average performance and cross-domain robustness (measured by coefficient of variation) for 64 model combinations. The Pareto frontier delineates the feasible region of optimal performance. Point size indicates model parameters, and colors represent transfer types.

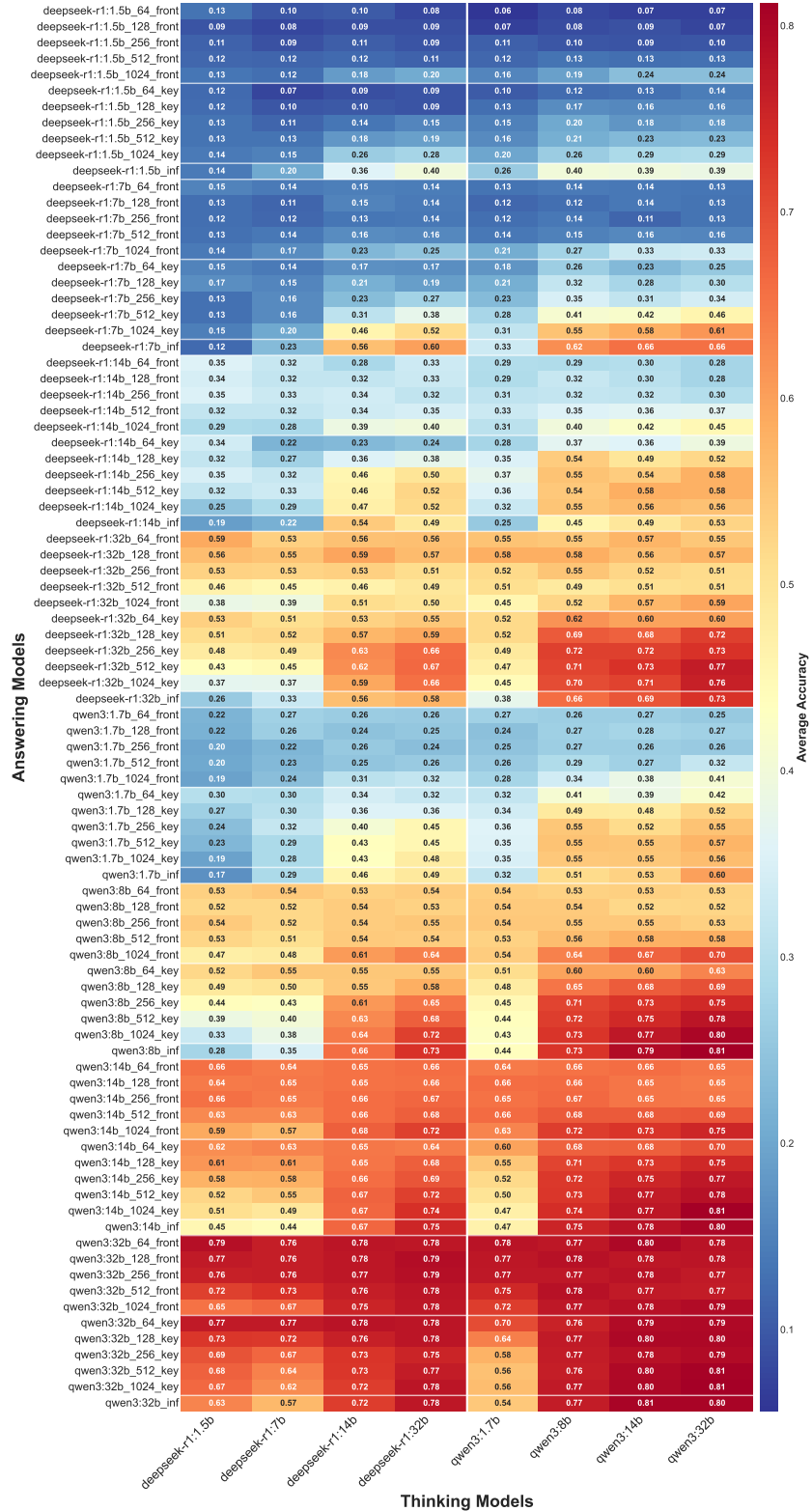


Figure 25: Performance matrix showing accuracy across all thinking–answering model combinations under different token budgets and compression strategies. Darker red indicates higher accuracy, with stronger diagonal patterns for same-family transfers.

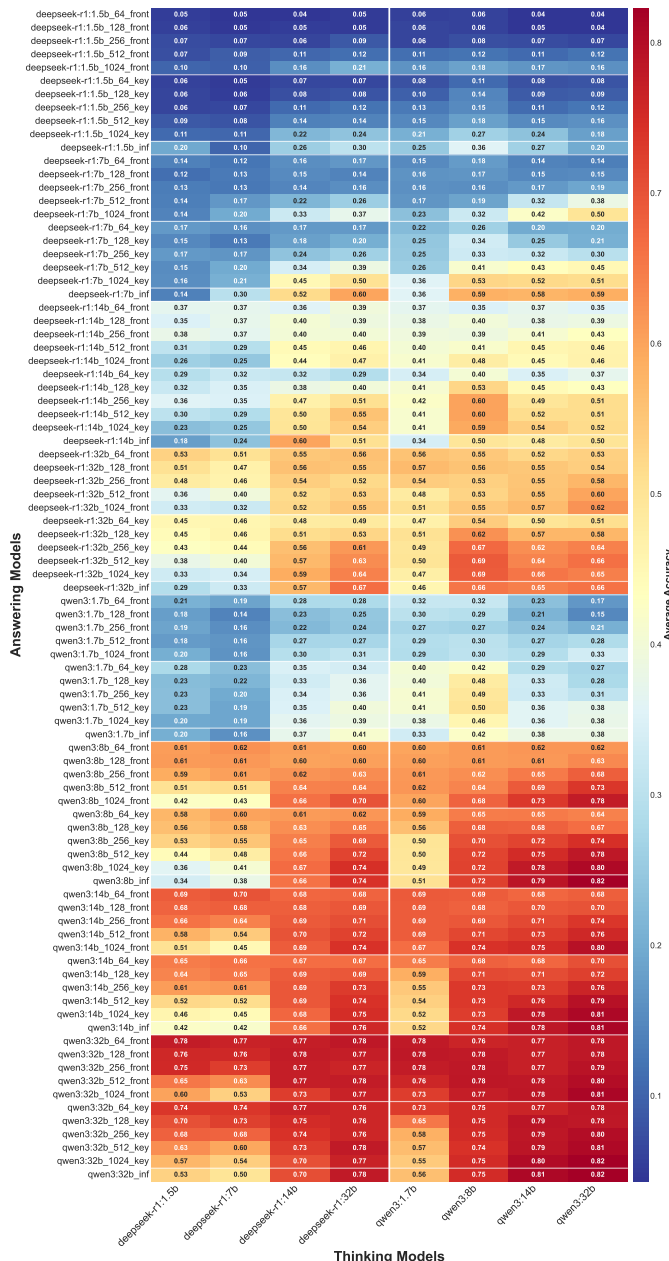


Figure 26: Performance matrix for the Chinese dataset showing accuracy across all thinking–answering model combinations under different token budgets. Diagonal patterns indicate architectural compatibility effects.

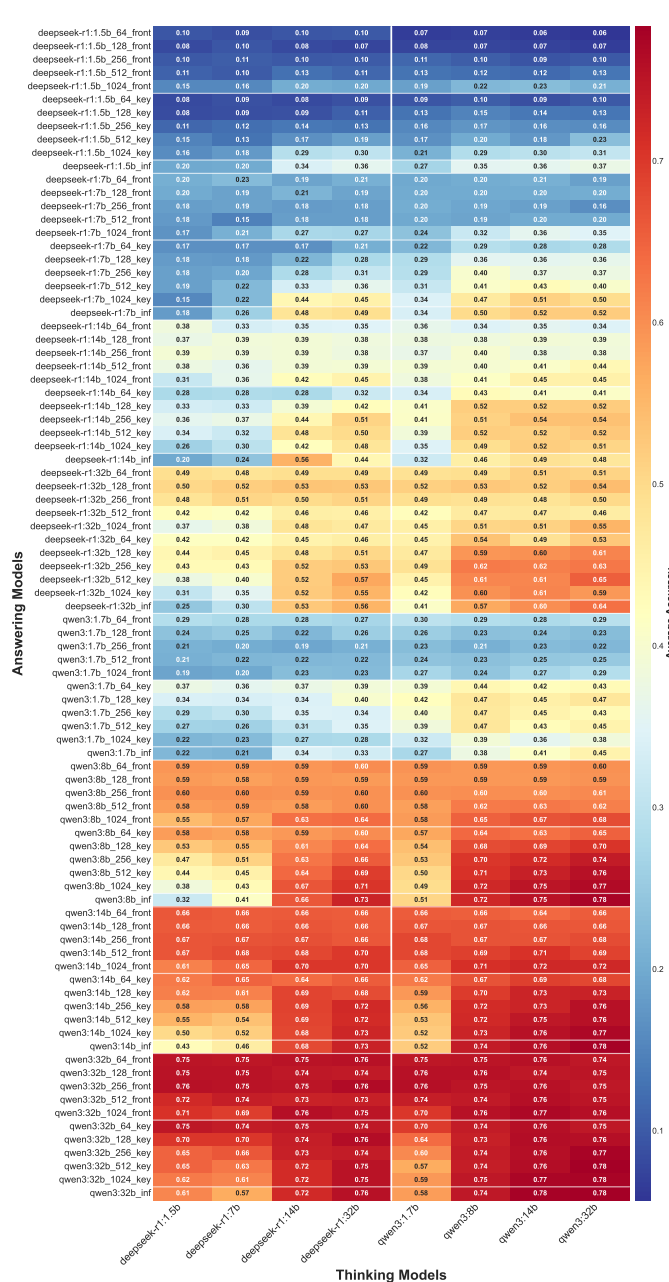


Figure 27: Performance matrix for the English dataset. The observed patterns are consistent with those from the Japanese and Chinese datasets.